

Signatures of Many-Body Localization in the Dynamics of Two-Level Systems in Glasses

Claudia Artiago,^{1,2,3,*} Federico Balducci,^{1,2,3,†} and Antonello Scardicchio^{2,3}

¹*SISSA, via Bonomea 265, 34136, Trieste, Italy*

²*The Abdus Salam International Center for Theoretical Physics, Strada Costiera 11, 34151, Trieste, Italy*

³*INFN Sezione di Trieste, Via Valerio 2, 34127 Trieste, Italy*

(Dated: July 6, 2022)

We investigate the quantum dynamics of Two-Level Systems (TLS) in glasses at low temperatures (1 K and below). We study an ensemble of TLSs coupled to phonons. By integrating out the phonons within the framework of the Gorini-Kossakowski-Sudarshan-Lindblad (GKSL) master equation, we derive the explicit form of the interaction among TLSs and of the dissipation terms. We find that the dynamics of the system shows clear signatures of many-body localization physics (in particular a power-law decay of the concurrence, which measures pairwise entanglement also in non-isolated systems) even in the presence of dissipation, if the latter is not too large. This feature can be ascribed to the presence of strong, long-tailed disorder characterizing the distributions of the model parameters. Our findings show that assuming ergodicity when discussing TLS physics might not be justified for all kinds of experiments on low-temperature glasses.

I. INTRODUCTION

Recent years have witnessed several advances in our understanding of the dynamics of many-body quantum systems. On one hand, the mechanism by which thermal equilibrium appears in isolated quantum systems has been explained via the Eigenstate Thermalization Hypothesis (ETH)[1–3], and its connection to the classic von Neumann ergodic theorem has been made clear [4]. On the other hand, a generic mechanism by which quantum systems can *avoid* going to thermal equilibrium has been identified in Many-Body Localization (MBL) [5–11]. Analogous phenomena take place in driven periodic systems (time crystals) [12–14], and in systems without disorder [15–23]. These progresses give now a more or less complete picture of the various ways of thermalization in quantum systems, under different conditions.

One of the places in which one routinely finds disorder *and* quantum effects at the same time is in the study of low-temperature properties of glasses. A series of classic experiments [24, 25] has made manifest that the properties of glasses at temperatures of 1K and below show a surprising degree of universality, and deviate significantly from Debye theory. Several theoretical ideas aimed at explaining these results, mostly on the lines of two seminal works [26, 27]. In those works, the idea of bi-stable tunnelling systems (or two-level systems, TLSs), whose parameters (energy difference and tunnelling rates) are very broadly distributed, was introduced. With an appropriate choice of these distributions, one could reproduce quantitatively the values of several equilibrium quantities, including specific heats, conductivity, and sound attenuation. The range of TLS models has been expanded considerably beyond the original works to account for

various experimental facts [28], and even criticized as a glorified curve-fitting procedure [29–31].

TLSs interact with phonons and, if they have an electric dipole moment, also with photons. Consequently, they also interact with one another, as it is confirmed by several experiments [32–37]. Interactions of TLSs and phonon (and photon) bath are also responsible for the equilibration of the TLSs at the bath temperature. Indeed, if the TLSs were not coupled, they would be just a set of local independent degrees of freedom, isolated from the environment.

The purpose of this paper is exactly to discuss, in view of the theoretical ideas born in the field of MBL, the mechanism for thermalization of TLSs coupled to phonons. We will idealize the system TLSs + phonons as an isolated system and — with some approximations — study the phenomenon of thermalization and the dynamics of entanglement among TLSs, and between TLSs and phonons. We will achieve this by deriving the Gorini-Kossakowski-Sudarshan-Lindblad (GKSL) equation for the reduced density matrix of the TLSs, tracing out the phonons. Note that the phonons of our system are delocalized (as should be the case for extremely low energy, even in disordered atoms arrangements)[38].

We focus in particular on entanglement creation and spreading as measured by the concurrence [39–41] and the entanglement entropy. The former measures the amount of entanglement between two TLSs; under time evolution it grows to a maximum, and then decays. The latter instead increases monotonically with time to reach a thermodynamic value. We study both an artificially isolated, coherent TLS system (only processes involving virtual phonons are considered), for which the effective Hamiltonian is MBL, and the open system (both virtual and real dephasing processes from coupling to phonons are considered). In the first case, we can confidently see the thermodynamic limit (our numerics goes up to $N = 60$ TLSs) and prove that the concurrence decays as a power-law in time $t^{-\beta_i}$, to a plateau value which

* cartiaco@sissa.it

† fbalducc@sissa.it

is exponentially small in the number of TLSs. This is typical of an MBL system. In the second case, the open system, we see that the concurrence decays indefinitely, again with a power-law $t^{-\beta_o}$, without ever reaching a plateau (the open system is effectively infinite). The exponents $\beta_{i,o}$ in the two scenarios are of the same order of magnitude. Their comparison shows that, within the statistical errors and finite-size corrections, β increases in the presence of dissipation.

The structure of the paper is as follows. In Sec. II, we introduce the Hamiltonian of the full system and comment on the various parameters that are needed to describe TLSs in amorphous media. In Sec. III, we integrate out the phonons, obtaining the GKSL equation for the TLS density matrix. We discuss the competition between interactions and dissipation, and sketch a dynamical phase diagram. In Sec. IV, we consider only the unitary part of the dynamics, and show what are the signatures of MBL on the entanglement quantifiers. In Sec. V, we introduce also the dissipation terms of the dynamics, and show how the results of Sec. IV change. Finally, in Sec. VI we summarize our results and indicate future research directions.

II. THE TLS MODEL

A. The Hamiltonian

We define the total Hamiltonian of the TLSs system and the thermal bath as [42–44]

$$H = H_{TLS} + H_B + H_{int}. \quad (1)$$

The phonon bath is described by

$$H_B = \sum_k \hbar \omega_k \psi_k^\dagger \psi_k,$$

ψ_k (resp., ψ_k^\dagger) being the annihilation (resp., creation) operator of a phonon with wavevector and polarization $k = (\mathbf{q}, \alpha)$. The dispersion relation in amorphous solids is, to a good approximation at low temperatures [45], $\omega_{\mathbf{q}\alpha} \simeq v_\alpha q$ with $v = v_L$ for longitudinal modes and $v = v_T$ for transverse modes [46]. Typically $v_L \simeq 1.6 v_T$; see Table I.

The TLS Hamiltonian is

$$H_{TLS} = \sum_i (\Delta_i \sigma_i^x + \varepsilon_i \sigma_i^z).$$

We use Pauli spins to represent the two states of a TLS; ε_i is the energy splitting and Δ_i the tunnelling amplitude in the i -th double-well. According to the original works [26, 27], we consider ε as drawn from a uniform distribution of width W :

$$p(\varepsilon) = \frac{1}{W} \Theta(W - \varepsilon) \Theta(\varepsilon) \quad (2)$$

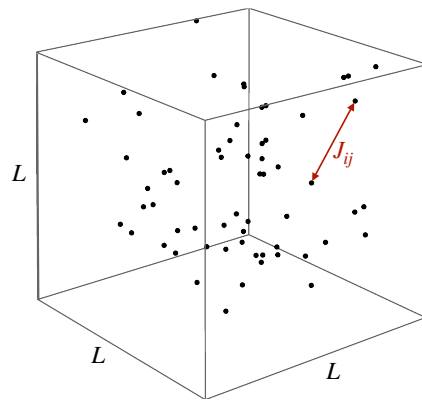


FIG. 1. The TLSs are uniformly distributed in a cube of size L , at constant density. Their pair interaction J_{ij} in Eq. (8) is mediated by phonons, that are also responsible for the dissipator in Eq. (10). We employ periodic boundary conditions to minimize finite-size effects.

(Θ is the Heaviside step function). The tunnelling amplitudes Δ_i are usually assumed to be very broadly distributed. The most reasonable distribution from a simplicity standpoint has been argued to be [26]

$$p_\Delta(\Delta) = \frac{\Theta(\Delta - \Delta_{min}) \Theta(\Delta_{max} - \Delta)}{\log(\Delta_{max}/\Delta_{min}) \Delta} \quad (3)$$

where

$$\Delta_{min} = \bar{\Delta} \cdot 10^{-n_\Delta/2}, \quad \Delta_{max} = \bar{\Delta} \cdot 10^{n_\Delta/2}$$

with n_Δ defining the span of the distribution: $\Delta_{max}/\Delta_{min} = 10^{n_\Delta}$. Since $\langle \log \Delta \rangle = \log \bar{\Delta}$, we note that $\bar{\Delta}$ is the typical value of the distribution.

The interaction Hamiltonian of the localized degrees of freedom with the strain field is, to lowest order [42–44],

$$H_{int} = \sum_{ik} \sigma_i^z (\xi_{ik} \psi_k + \text{h.c.}), \quad (4)$$

with

$$\xi_{jk} = -i \sqrt{\frac{\hbar}{2V\rho\omega_k}} \gamma_j D_j^{ab} e_k^{ab} e^{i\mathbf{q}\cdot\mathbf{r}_j}, \quad (5)$$

where ρ is the material density, V the volume, $\gamma_j D_j^{ab}$ the elastic dipole tensor of the j -th TLS (the strength γ_j has the dimension of an energy and D_j^{ab} is dimensionless), and $e_k^{ab} := \frac{1}{2}(q^a \hat{e}_k^b + q^b \hat{e}_k^a)$ (\mathbf{q} is the wavevector and \hat{e}_k the unit (\mathbf{q}, α) -polarization vector).

B. Disorder distributions of the parameters

In the literature, most of the parameters defining the Hamiltonian in Eq. (1) are drawn from very wide probability distributions, which span several orders of magnitude and overlap one with another. In Table I we provide

	SiO ₂	BK7	PMMA
W [meV]	130	70	30
Δ_{max} [meV]	13	7	3
$\overline{\Delta}$ [meV]	10^{-3}	10^{-3}	10^{-4}
Δ_{min} [meV]	10^{-7}	10^{-7}	10^{-8}
γ_i [eV]	0.8	0.7	0.3
ρ [g/cm ³]	2.2	2.5	1.2
v_L [km/s]	5.8	6.2	3.2
v_T [km/s]	3.8	3.8	1.6
$k_B T_D$ [meV]	30	30	10
ρ_{TLS} [nm ⁻³]	0.3	0.2	0.05
$\hbar\tau^{-1}$ [meV]	1.8	1.7	0.45

TABLE I. Summary of the model parameters for fused quartz (SiO₂), borosilicate glass (BK7), and plexiglass (PMMA). The parameters v_L, v_T, ρ and the Debye temperature T_D are independent; their values are derived from experimental measurements [44, 47]. One can reasonably assume $W \approx k_B T_{glass}$: indeed the TLSs are formed at the glass transition [25]. As a consequence, one should also set $\Delta_{max} \approx 10^{-1} W$ in order to have a density of states that goes to zero above W [26], and $\Delta_{min} \approx 10^{-9} W$ to reproduce instead a flat DOS at low temperatures [48]. The precise value of Δ_{max} and Δ_{min} is not crucial, since they enter only logarithmically in the quantities of interest. One can obtain the numerical density of the TLSs ρ_{TLS} from the experimentally measurable parameter $\bar{P} = \rho_{TLS}/W \log(\Delta_{max}/\Delta_{min})$ [25, 47]. The experimental values of γ_i are taken from [47].

a list of such experimental parameters for three glassy materials.

In our numerical simulations we employ less broad distributions, for which it is possible to disentangle the different contributions to the dynamics. We argue that this choice, if properly taken, does not qualitatively alter the physical content and the predictions of the model.

In previous works [25], the width W of the uniform distribution of the energy splittings (see Eq. (2)) is usually considered of order 0.1 eV. We fix $W \equiv 1$, thus setting the energy scale.

As for the tunnelling amplitudes Δ_i (Eq. (3)), it is typically considered that $n_\Delta \simeq 8$ and $\overline{\Delta}/W \approx 10^{-5}$, making $p_\Delta(\Delta)$ very wide. For numerical convenience (in particular, the smallness of the accessible system sizes), we set $\overline{\Delta}/W = 10^{-1}$, unless otherwise specified, and $n_\Delta = 2$.

The probability distributions of the TLS-phonon coupling strengths γ_i and of the (dimensionless) elastic dipole tensors D_i^{ab} are induced by the distributions of the shapes and the directions of the TLSs in space. In the literature [25, 28], it is argued that γ_i should be of the same order of magnitude of W , since the former is related to the energy shift induced in a TLS by a phonon, and it must be comparable with the energy imbalance of the two minima in the double-well. Therefore, for simplicity, we set $\gamma_i \equiv W$, absorbing in the dipoles D_i^{ab} all the disorder fluctuations: they become random variables of order 1. We will not specify the full distribution of

their entries, since in Secs. IIIB1–IIIB2 we will show that only some combinations of the entries are needed. We refer to those Sections for more details.

For the numerical simulations, we also fix the material density as $\rho = 2$ g/cm³, and the speed of sound in glasses as $v_{L,T} = 5$ km/s, irrespective of the polarization.

Finally, we consider the TLSs as uniformly distributed in a cube with side L , and compute their distances r_{ij} using periodic boundary conditions. The cube side depends on the number of TLSs as $L = L_0 N^{1/3}$, with $L_0 \sim \rho_{TLS}^{-1/3}$, so that we keep fixed the TLS number density ρ_{TLS} . For numerical purposes, we fix $L_0 \simeq 10$ nm (as often done in the literature [28]) and perform all of our simulations by rescaling $L_0 \rightarrow L_0/R$ with $R = 10^3$, (see Sec. IIIB2). The parameter R enhances the interactions and enables us to explore the dynamical phase diagram of Fig. 2.

With these choices of the parameters, the on-site frequencies ν_i , the TLS-TLS interactions, and the decoherence terms are of comparable orders of magnitude. Our results will be discussed in view of this competition.

III. THE GKSL MASTER EQUATION

To study the dynamics of the TLSs, we integrate out the phonons. This can be done at several degrees of approximation, depending on the assumptions made. We study the system in the framework of the GKSL master equation [49] (reviewed in App. A to fix the notation), thus working in the weak-coupling limit, whose validity has to be checked a posteriori.

Besides weak coupling, the GKSL framework implies three further simplifications: the Born approximation, the Markov approximation and the rotating-wave approximation. In the first one, one assumes that at all times the influence of the TLSs on the phonon thermal population is negligible. This is a consequence of weak-coupling, and of the TLSs being a dilute system in the (amorphous) lattice. Therefore, we expect the Born approximation to be valid to a good extent. The Markov approximation instead entails that all the bath excitations decay on a very fast timescale w.r.t. that of the TLSs. This is not guaranteed when working at ultra-low temperatures, but it is still a good starting point. Finally, we employ the rotating wave approximation which is more subtle for our particular system. It consists in considering the typical dynamical timescale of the *isolated* system $\tau_i \ll \tau_o$, where τ_o is the relaxation time of the *open* system. This results in TLS-TLS interactions that commute with the single TLS Hamiltonian, simplifying the many-body physics w.r.t. other models used in the literature, and ultimately leading to MBL. However, because of the strong, long-tailed disorder distributions usually assumed for the TLS model, we considered the rotating-wave approximation to be valid.

In further studies, it might be interesting to go beyond the GKSL master equation, and relax its assumptions.

A. The free TLS eigenoperators

To apply the GKSL formalism to the Hamiltonian in Eq. (1), we note that each TLS is coupled via σ_i^z to the environment operator $E_i \equiv \sum_k (\xi_{ik}\psi_k + \xi_{ik}^*\psi_k^\dagger)$. To proceed, one has to find the operator decomposition of σ_i^z that evolves trivially under the free dynamics of a single TLS: $[H_{TLS}, S_i^\nu] = -\hbar\nu S_i^\nu$ (see App. A for more details). Solving the 2×2 eigenvalue problem, one finds the eigenfrequencies

$$\nu_0 = 0, \quad \nu_\pm = \pm \frac{2}{\hbar} \sqrt{\varepsilon^2 + \Delta^2}.$$

and the corresponding eigenoperators

$$S_i^0 = \vec{v}_{i,0} \cdot \vec{\sigma}_i, \quad S_i^\pm = \vec{v}_{i,\pm} \cdot \vec{\sigma}_i,$$

where $\vec{v}_0 = -\frac{2}{\hbar\nu}(\Delta, 0, \varepsilon)$ and $\vec{v}_\pm = \frac{2}{\hbar\nu}(-\varepsilon, \pm i\hbar\nu/2, \Delta)$. The operators S_i^μ are normalized in such a way that they obey the same algebra of the Pauli matrices. The free

TLS Hamiltonian reads

$$H_{TLS} = -\frac{1}{2} \sum_i \hbar\nu_i S_i^0.$$

Note that, because of our choice of parameters (Sec. II B), $\hbar\nu_i$ will be typically of order W .

B. Coupling to phonons

The coupling with phonons induces both dissipation and TLS–TLS interactions. The phonons are assumed to be in a thermal state ρ_B^T at all times, therefore they are not influenced by being coupled to the TLSs. Under such assumption, the strengths of dissipation and interactions are quantified by (see App. A)

$$\Gamma_{ij}^\nu = \frac{1}{\hbar^2} \int_0^\infty ds e^{i\nu s} \text{Tr}_B \left[\rho_B^T \hat{E}_i^\dagger(t) \hat{E}_j(t-s) \right].$$

The time-evolved environment operators are found upon using the canonical commutation relations:

$$\hat{E}_i(t) = \sum_k (\xi_{ik} e^{-i\omega_k t} \psi_k + \xi_{ik}^* e^{i\omega_k t} \psi_k^\dagger).$$

It follows

$$\begin{aligned} \hbar^2 \Gamma_{ij}^\nu &= \int_0^\infty ds e^{i\nu s} \text{Tr}_B \left\{ \rho_B^T \sum_{kl} (\xi_{ik} e^{-i\omega_k t} \psi_k + \text{h.c.}) (\xi_{jl} e^{-i\omega_l(t-s)} \psi_l + \text{h.c.}) \right\} \\ &= \int_0^\infty ds e^{i\nu s} \sum_k \left\{ \xi_{ik} \xi_{jk}^* e^{-i\omega_k s} \text{Tr}_B [\rho_B^T \psi_k \psi_k^\dagger] + \xi_{ik}^* \xi_{jk} e^{i\omega_k s} \text{Tr}_B [\rho_B^T \psi_k^\dagger \psi_k] \right\} \\ &= \int_0^\infty ds e^{i\nu s} \sum_k \left[\xi_{ik} \xi_{jk}^* e^{-i\omega_k s} (f_T(\hbar\omega_k) + 1) + \xi_{ik}^* \xi_{jk} e^{i\omega_k s} f_T(\hbar\omega_k) \right] \end{aligned}$$

where we introduced the Bose-Einstein distribution function at temperature T : $f_T(\varepsilon) := (e^{\varepsilon/k_B T} - 1)^{-1}$. We perform the time integral, using the identity $\int_0^\infty ds e^{i\zeta s} = i \text{PV} \frac{1}{\zeta} + \pi \delta(\zeta)$. From Eqs. (4)–(5), we arrive at

$$\begin{aligned} \Gamma_{ij}^\nu &= \frac{\gamma_i \gamma_j}{8\rho} \sum_{abcd} D_i^{ab} D_j^{cd} \sum_\alpha \int \frac{d^3 q}{(2\pi)^3} \frac{1}{\hbar\omega_k} (q^a \hat{e}_k^b + q^b \hat{e}_k^a) (q^c \hat{e}_k^d + q^d \hat{e}_k^c) \\ &\quad \times \left[(f_T(\hbar\omega_k) + 1) \left(i \text{PV} \frac{1}{\nu - \omega_k} + \pi \delta(\nu - \omega_k) \right) e^{i\mathbf{q} \cdot (\mathbf{r}_i - \mathbf{r}_j)} \right. \\ &\quad \left. + f_T(\hbar\omega_k) \left(i \text{PV} \frac{1}{\nu + \omega_k} + \pi \delta(\nu + \omega_k) \right) e^{-i\mathbf{q} \cdot (\mathbf{r}_i - \mathbf{r}_j)} \right]. \quad (6) \end{aligned}$$

1. The decoherence rates

The decoherence rates Y_{ij}^ν can be obtained from the real part of Γ_{ij}^ν (App. A, Eq. (A12)). One can set the

two-site rates $Y_{i \neq j}^\nu = 0$ because, in view of the wideness of the frequency distribution, it is very unlikely to have two TLSs with equal eigenfrequencies $\nu_i = \nu_j$. Moreover, one has $Y_{ii}^0 = 0$ because the phonon density of states at zero frequency vanishes. Thus, the only surviving terms

are Y_{ii}^{\pm} .

The rates can be found after the lengthy but straightforward calculation reported in App. B. Defining

$$Y_i := \frac{\gamma_i^2 \Delta_i^2 (\hbar \nu_i)}{30\pi \rho \hbar^4} \left[\frac{\langle\langle D_i D_i \rangle\rangle_{\Upsilon, L}}{v_L^5} + \frac{\langle\langle D_i D_i \rangle\rangle_{\Upsilon, T}}{v_T^5} \right]$$

where the $\langle\langle D_i D_i \rangle\rangle_{\Upsilon, \alpha}$ represent angular averages of the dimensionless dipole moments (see App. B), we have

$$Y_{ii}^+ = Y_i (f_T(\hbar \nu_i) + 1), \quad Y_{ii}^- = Y_i f_T(\hbar \nu_i). \quad (7)$$

Having set $\hbar \nu_i \sim W \sim 0.1$ eV, at temperature $T \sim 1$ K and below our system is effectively at *zero temperature*. Thus, one can neglect the contribution of the Bose-Einstein distribution function, obtaining

$$Y_{ii}^+ \approx Y_i, \quad Y_{ii}^- \approx 0.$$

As anticipated in Sec. II B, instead of drawing the single matrix elements of the dipole moments D_i^{ab} , we will directly extract the scalars $\langle\langle D_i D_i \rangle\rangle_{\Upsilon, \alpha}$. Since, by construction, they must be positive, we take them to be the square of a Gaussian variable: $\langle\langle D_i D_i \rangle\rangle_{\Upsilon, \alpha} \sim \chi_1^2$ (i.e., the chi-square distribution), irrespective of polarization.

Considering the typical values of the disorder distributions, the numerical estimate of the dissipation rates gives $\hbar Y_i / W \sim 10^{-9}$, justifying a posteriori the weak-coupling approximation.

2. The Lamb-Stark shift Hamiltonian

Tracing out the phonons generates also TLS–TLS interactions. In the GKSL framework, they commute with the free TLS evolution, and represent the Stark and Lamb shifts contributions (Eq. (A11)). In App. C, we show that the predominant channel for the interactions is induced by the rotating-wave approximation, which forces $\nu_i = \nu_j$ and this condition is satisfied only for $\nu = 0$. Thus, the Lamb-Stark Hamiltonian reads

$$H_{LS} = \sum_{ij} J_{ij} S_i^0 S_j^0,$$

where the interaction strengths J_{ij} can be obtained from the imaginary part of Γ_{ij}^0 (see Eq. (A13) and App. C):

$$J_{ij} = -\frac{1}{8\pi \rho r_{ij}^3} \frac{\gamma_i \varepsilon_i}{\hbar \nu_i} \frac{\gamma_j \varepsilon_j}{\hbar \nu_j} \times \left[\frac{\langle\langle D_i D_j \rangle\rangle_{\Pi, L}}{v_L^2} + \frac{\langle\langle D_i D_j \rangle\rangle_{\Pi, T}}{v_T^2} \right]. \quad (8)$$

In the above equation, the terms $\langle\langle D_i D_j \rangle\rangle_{\Pi, \alpha}$ are again angular averages of the dipole moments, as the ones in Eq. (7) (see App. C for more details). For our purposes, we will assume them to be normally distributed: $\langle\langle D_i D_j \rangle\rangle_{\Pi, \alpha} \sim \mathcal{N}(0, 1)$, irrespective of polarization; therefore, J_{ij} can be either positive or negative.

The interactions between TLSs are responsible for dephasing in the unitary time-evolution. If one artificially turns off the jump operators, i.e. they set the decoherence rates $Y_i \equiv 0$, diffusive transport is suppressed (since the Hamiltonian commutes with S_i^0), but the entanglement spreading persists. As we will see in the next Section, in this case, the entanglement can grow indefinitely due to the interaction-induced dephasing, as in canonical MBL systems, and the concurrence decays as a power law in time.

Note that, since we have effectively removed the temperature contribution, the typical relative strength of the dissipation and interaction terms is

$$\frac{\hbar Y_i}{J_{ij}} \sim \left(\frac{\bar{\Delta}}{W} \right)^2 \left(\frac{W}{\hbar \tau^{-1}} \right)^3. \quad (9)$$

where $\tau = r/v$, with r the typical distance between TLSs and v the speed of sound in the glass. If the typical timescale of interaction is short w.r.t. the typical timescale of dissipation, the signatures of an MBL transient regime can be observed in the dynamics of the system, and in particular in the spreading of entanglement. In Fig. 2, we show a tentative dynamical phase diagram for the system.

Recalling that in experiments $\bar{\Delta} \sim 10^{-5} W$ while $W \sim 0.1$ eV and, considering $v \sim 5$ km/s and $r \sim 10$ nm, we have $\hbar \tau^{-1} \sim 1$ meV. Thus, the ratio is approximately $\hbar Y / J \sim 10^{-5} \div 10^{-4}$, making dissipation much slower than the interaction part of the unitary dynamics. Even if one allows $\bar{\Delta}$ — the most difficult parameter to infer from experiments — to vary of an order of magnitude, the system will still present an MBL transient regime.

In order to explore the phase diagram given by the GKSL master equation, and considering the parameter choices of Sec. II B, we compute Eq. (8) scaling the average distance of the TLSs by a factor R^{-1} with $R > 1$, i.e. we substitute $r_{ij} \rightarrow r_{ij}/R$. This effectively changes the interactions by a factor by R^3 .

C. The full GKSL equation

Combining the results obtained in the previous Sections, the GKSL equation is

$$\begin{aligned} \partial_t \rho(t) = & -\frac{i}{\hbar} [H_{TLS} + H_{LS}, \rho(t)] \\ & + \sum_i Y_i f_T(\hbar \nu_i) [S_i^+ \rho(t) S_i^- + S_i^- \rho(t) S_i^+ - 4\rho(t)] \\ & + \sum_i Y_i [S_i^+ \rho(t) S_i^- + \{\rho(t), S_i^0\} - 2\rho(t)], \end{aligned} \quad (10)$$

which can be rewritten in terms of jump superoperators \mathcal{L}_i as

$$\partial_t \rho(t) = -\frac{i}{\hbar} [H_{TLS} + H_{LS}, \rho(t)] + \sum_i \mathcal{L}_i \rho(t).$$

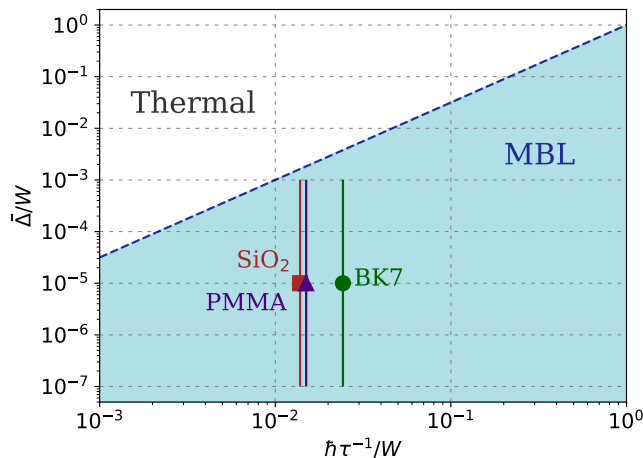


FIG. 2. Sketch of the expected phase diagram for TLSs in glasses. From Eq. (9) we see that an MBL transient regime can be observed before thermalization takes place, if the typical timescales of interaction are short w.r.t. the dissipation timescales (blue-shaded area). The three glassy materials reported in Table I lie well within the MBL region, even accounting for the large uncertainties in the parameter $\bar{\Delta}$ (the standard deviation of $\log(\Delta_i)$ is plotted as an errorbar). Thus, the localized regime should be experimentally observable.

This constitutes the starting point for exploring the quantum dynamics of TLSs.

First, we notice that, in the absence of dissipation, the evolution would be unitary, governed by the Hamiltonian

$$H_{TLS} + H_{LS} = -\frac{1}{2} \sum_i \hbar \nu_i S_i^0 + \sum_{ij} J_{ij} S_i^0 S_j^0. \quad (11)$$

$H_{TLS} + H_{LS}$ has precisely the form of a *l-bit Hamiltonian*, typical of MBL systems. In other words, the value assumed by each S_i^0 is conserved by the dynamics: they are Local Integrals Of Motion (or LIOMs) [8, 50–54]. However, this Hamiltonian term of the TLS dynamics presents two main differences with respect to the typical effective Hamiltonian in MBL systems. First, these l-bits are formed by *single* spins, not exponentially localized groups of them. Second, the interaction between the l-bits decays with distance as a power law rather than exponentially: $J_{ij} = J(r_{ij}) \propto r_{ij}^{-3}$. However, we will show that these differences do not qualitatively alter the behavior of entanglement.

The picture described so far is broken by the introduction of the jump operators governing dissipation and decoherence. On one hand, dissipating terms in the GKSL equation kill long-time coherence because they drive the system to a thermal phase. On the other hand, our particular Lindbladian contains the operators S_i^+ and S_i^- , which do not commute with the LIOMs S_i^0 , and cause non-trivial dynamics even at shorter times.

We note that, in some previous works [28, 55, 56], the flip-flop operators ($S_i^+ S_j^- + \text{h.c.}$) and ($S_i^+ S_j^+ + \text{h.c.}$) are

introduced in the Hamiltonian by general arguments. However, according to our derivation and many other studies [42–44, 57], we will restrict the analysis to the Hamiltonian in Eq. (11) (see App. D for more details).

In the following, we introduce a factor $\epsilon \leq 1$ to artificially tune the strength of the jump operators in the Lindbladian equation:

$$\partial_t \rho(t) = -\frac{i}{\hbar} [H_{TLS} + H_{LS}, \rho(t)] + \epsilon \sum_i \mathcal{L}_i \rho(t). \quad (12)$$

In this way, by changing ϵ we can interpolate between the coherent MBL dynamics and the one including dissipation.

IV. UNITARY EVOLUTION OF THE TLS

This Section is entirely devoted to the study of the time evolution of a system of N TLSs governed by the Hamiltonian (11). The initial state of the dynamics is a product state in which each TLS is a unit random vector on the Bloch sphere. Thus, the system is initially at infinite temperature. The Hamiltonian (11) is in the l-bit form, i.e. the values assumed by the operators S_i^0 are local integrals of motion, as discussed in Sec. III C. Studying the dynamics induced only by the Hamiltonian term is equivalent to set $\epsilon = 0$ in the GKSL equation (12), i.e. to assume that the timescales of decoherence/dissipation are much longer than those of the interactions, and a coherent many-body dynamics can take place before thermal equilibrium is reached. This situation corresponds to the MBL phase depicted in the phase diagram of Fig. 2.

The assumption that the initial state is factorized allows us to track precisely the entanglement growth and spreading. The choice of the appropriate entanglement measure is not obvious: since we are dealing with an open quantum system, we want such measure to discriminate between quantum entanglement and thermal entropy. A reliable measure of (pairwise) quantum entanglement in open systems is the *concurrence* C_{ij} [39–41], where i and j are TLS indices. The concurrence quantifies the distance of the two-site reduced density matrix ρ_{ij} from the manifold of mixed, separable states, which have the form $\rho = \sum_a p_a \rho_a^{sep}$ where ρ_a^{sep} are separable, and $p_a \geq 0$. This implies that, if $C_{ij} > 0$, there is no mixture of separable states that can account for the correlations between sites i and j . It can be shown [41] that $C_{ij} = \max\{0, \lambda_1 - \lambda_2 - \lambda_3 - \lambda_4\}$ where λ_a^2 are the eigenvalues of the matrix $R_{ij} = \rho_{ij}(\sigma_y \otimes \sigma_y) \rho_{ij}^*(\sigma_y \otimes \sigma_y)$ sorted in descending order.

It is known that in MBL systems the concurrence decays in time as a power-law [58], the exponent depending on the details of the Hamiltonian. In general, power-law decays of correlation functions are known [59] to be a feature of MBL dynamics, and the concurrence (albeit not

an operator nor a correlation function) follows the same rule. We find that this is valid in the case of TLSs as well, even though the Hamiltonian governing the unitary dynamics, $H_{TLS} + H_{LS}$, is different from the standard 1-bit Hamiltonian of MBL systems, as pointed out in Sec. III C.

Its particular definition allows the concurrence to quantify the entanglement between the two TLSs considered, irrespective of how they are entangled with other degrees of freedom. Thus, it spots entanglement between two TLSs even if they are thermal, i.e. also entangled with a bath. For this reason, we can employ the concurrence as a well-defined entanglement measure also in the presence of dissipation, as we will do in Sec. V.

In the rest of this Section, we will discuss how we performed the numerical simulations of a group of N TLSs evolving according to the Hamiltonian (11), and the results we obtained. Thanks to the diagonal nature of the Hamiltonian and the choice of initial product states, few-sites observables are efficient to compute, as was recognized in previous studies [58–60]. It is not necessary to

perform the time evolution of the whole $2^N \times 2^N$ density matrix, but only to carry out $O(N)$ operations. In this way, we could easily simulate a system of $N = 60$ TLSs.

To illustrate the idea, we show how to compute the two-site density matrix ρ_{ij} with $O(N)$ steps. Call the initial density matrix

$$\rho_0 = \bigotimes_{i=1}^N \rho_{0,i} = \bigotimes_{i=1}^N \sum_{s_i, s'_i} \rho_{0,i}^{s_i s'_i} |s_i\rangle \langle s'_i|.$$

Time evolving the density matrix according to the von Neumann equation and rearranging the sum:

$$\rho(t) = \sum_{s, s'} \prod_i \rho_{0,i}^{s_i s'_i} |s\rangle \langle s'| e^{-i(H[s] - H[s'])t/\hbar}$$

where $H[s] = -\frac{1}{2} \sum_i \hbar \nu_i s_i + \sum_{ij} J_{ij} s_i s_j$, with $s_i = \pm 1$ projection of the spin-1/2 on the 0-axis. Without loss of generality, we can trace out all the spins but the first two. The matrix elements of the two-site reduced density matrix read

$$\begin{aligned} \langle s_1 s_2 | \rho_{12}(t) | s'_1 s'_2 \rangle &= \langle s_1 s_2 | \text{Tr}_{3\dots N} \rho(t) | s'_1 s'_2 \rangle \\ &= \sum_{s_3 \dots s_N} \rho_{0,1}^{s_1, s'_1} \rho_{0,2}^{s_2, s'_2} \rho_{0,3}^{s_3, s_3} \dots \rho_{0,N}^{s_N, s_N} e^{-i(H[s_1 s_2 s_3 \dots s_N] - H[s'_1 s'_2 s_3 \dots s_N])t/\hbar} \\ &= \rho_{0,1}^{s_1, s'_1} e^{-i\Delta H_{12}[s]t/\hbar} \rho_{0,2}^{s_2, s'_2} \prod_{j=3}^N \left[\rho_{0,j}^{\uparrow, \uparrow} e^{-i\Delta H_{12j}[s]t/\hbar} + \rho_{0,j}^{\downarrow, \downarrow} e^{i\Delta H_{12j}[s]t/\hbar} \right] \end{aligned}$$

where $\Delta H_{12}[s] := 2J_{12}(s_1 s_2 - s'_1 s'_2) - \frac{\hbar \nu_1}{2}(s_1 - s'_1) - \frac{\hbar \nu_2}{2}(s_2 - s'_2)$ and $\Delta H_{12j}[s] := 2J_{1j}(s_1 - s'_1) + 2J_{2j}(s_2 - s'_2)$.

An analogue procedure gives the k -site reduced density matrix with $O(k^2 N)$ steps. Thus, when one is interested in few-sites observables this technique permits to simulate systems of very large size.

The results of our simulations for the quantity

$$C(t) \equiv \frac{1}{N} \sum_{1 \leq i < j \leq N} C_{ij}(t) \quad (13)$$

are shown in Figs. 3, 4, and 5. The normalization factor $1/N$ in the definition of $C(t)$ (instead the seemingly natural $1/N^2$) is due to the *monogamy of entanglement*. Each TLS can be highly entangled only with another TLS, so among the $N(N-1)/2$ terms in the sum, only $O(N)$ will be non-negligible.

One can see that the concurrence raises linearly from the initial value 0 (the initial state is factorized) to a value independent of N (but slightly dependent on $\bar{\Delta}$).

It then falls to a plateau through a power-law decay:

$$C(t) \sim \begin{cases} t & \text{if } t < t_1, \\ t^{-\beta_i} & \text{if } t_1 < t < t_2, \\ e^{-\alpha N} & \text{if } t > t_2. \end{cases}$$

whose exponent β_i depends on $\bar{\Delta}$. We found that t_1 does not depend on N significantly but t_2 grows with N and diverges in the thermodynamic limit.

The behavior of the concurrence can be compared with the half-system entanglement entropy (HSEE), that we call S_E . Since the system is three-dimensional, and the TLSs do not fall on a regular lattice, we decided to bipartite the system in the following way. For each TLS, a bubble is constructed around it so that $N/2$ TLSs fall inside and $N/2$ outside the bubble. The entanglement entropy relative to the bipartition is computed, and then averaged over all such bipartitions. The results are shown in Fig. 6, compared with the behavior of $C(t)$. We see that $S_E(t)$ increases monotonically until it reaches a plateau roughly proportional to N , indicating a volume law. Indeed, while the concurrence reaches its maximum on a

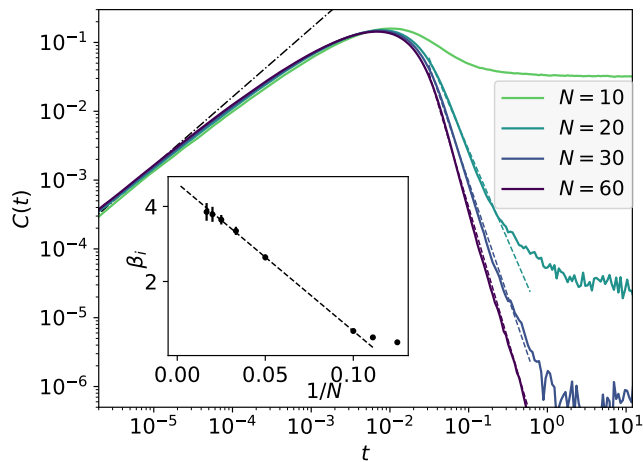


FIG. 3. Average concurrence for unitary dynamics (solid lines). After a linear raise $C \sim t$ (black dashed-dotted line), the average concurrence decays with a power-law $C \sim t^{-\beta_i}$ (dashed lines), in accordance with MBL theory, down to a value which is exponentially small in N . We set $\overline{\Delta} = 0.1$, $R = 10^3$; the results are averaged over 5000 disorder realizations. *Inset:* The exponent β_i depends on N and reaches a finite value in the thermodynamic limit. The errors are computed by using the statistical uncertainties of the concurrence values. Not all datasets were shown in the main figure to improve readability.

timescale of order $\sim \hbar/J_{ij}$ and then decreases because of the spreading of the entanglement among many TLSs, the entanglement entropy keeps growing. From our data, the HSEE seems to be growing logarithmically in time, even though the usual arguments for MBL[8, 61] should not apply for our long-range, $3d$ interactions.

V. INTRODUCING THE DISSIPATION

This Section is devoted to the study of the time evolution of the TLS system governed by the GKSL master equation (12), rewritten here for readability:

$$\partial_t \rho(t) = -\frac{i}{\hbar} [H_{TLS} + H_{LS}, \rho(t)] + \epsilon \sum_i \mathcal{L}_i \rho(t).$$

We will consider $\epsilon \neq 0$, i.e. the system will be in the presence of dissipation and decoherence. Increasing ϵ , we increase the typical dissipation rate. For our particular choice of parameters (Sec. IIB), when $\epsilon = 1$, it ultimately becomes comparable with the timescale of the interactions J_{ij} .

To investigate the time evolution of the system, one has to integrate numerically the GKSL master equation for the TLS density matrix (see App. F for more details). In this way, we could access systems up to $N = 9$; indeed, because of the doubling of the Hilbert space dimension, we are forced to these very small system sizes. In the

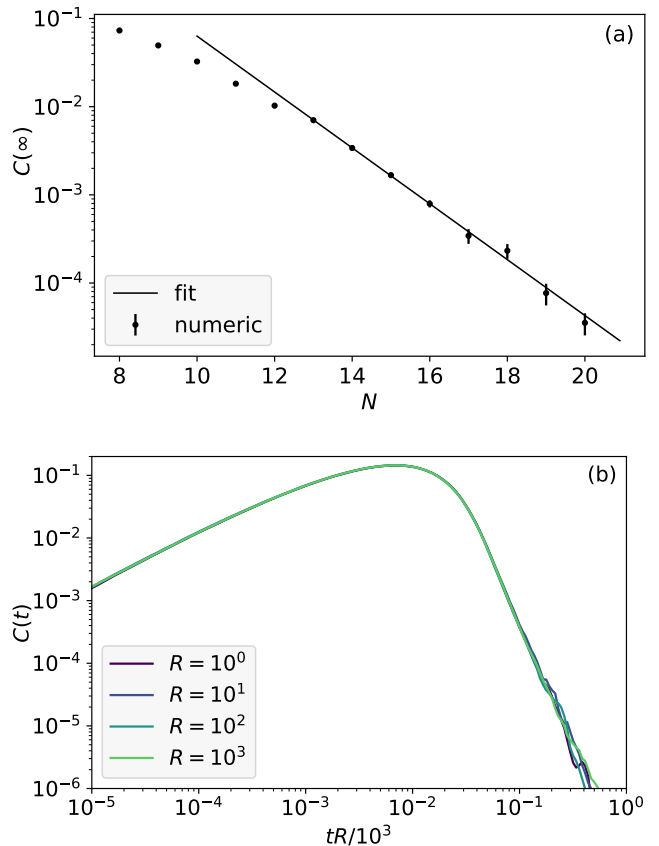


FIG. 4. Results for $\epsilon = 0$. (a) Plateau value of the average concurrence at long times (dots), with errors coming from statistical fluctuations. From a fit (solid line) we find that $C(\infty) \propto e^{-\alpha N}$ with $\alpha \approx 0.73$. This is considerably larger than the value given by the ETH prediction, i.e. a random state, which obeys $C \propto e^{-a2^N}$ with $a \approx 0.127$ (see App. E). Here $R = 10^3$, $\overline{\Delta} = 0.1$, and an average over at least 1000 disorder realizations was performed. (b) Average concurrence for different interaction strengths R . Rescaling the time as $t \rightarrow tR/10^3$ (we normalize to $R = 10^3$ to compare to the other plots) we see that the curves collapse, showing that the value of R only shifts the timescale but does not modify the shape of the curve $C(t)$. Here $N = 50$, $\overline{\Delta} = 0.1$, and an average over 1000 disorder realizations was performed.

following analyses, we varied both N (to perform a finite-size scaling) and ϵ .

As can be seen from Fig. 7, when ϵ is small enough the concurrence $C(t)$ reaches its maximum at the same time as with unitary dynamics ($\epsilon = 0$). Then, it decays from such peak and stabilizes around a finite value dependent on N (see Sec. IV), following the same behavior as in the case $\epsilon = 0$. Ultimately, the dissipation forces $C(t)$ to vanish; $C(t)$ departs from the $\epsilon = 0$ plateau, $C(\infty; \epsilon = 0)$, with a stretched-exponential functional form (Fig. 8). We can ascribe this feature to the interaction between TLSs and phonons: when $\epsilon \neq 0$, thanks to the dissipative terms in the GKSL equation (Eq. 12), entanglement can

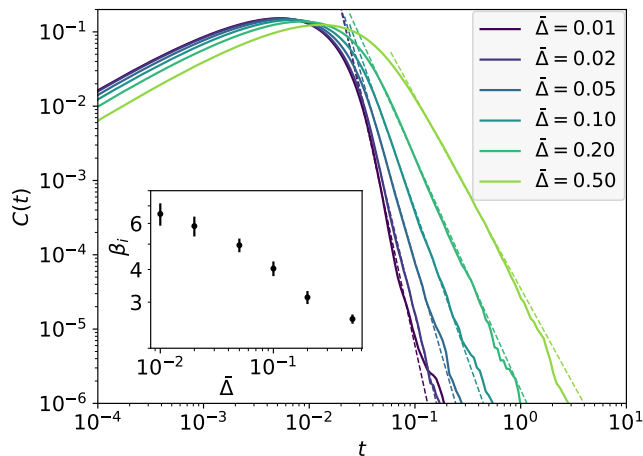


FIG. 5. Dependence of the concurrence decay exponent β_i on $\bar{\Delta}$ in the case of unitary evolution ($\epsilon = 0$). We set $N = 50$, $R = 10^3$ and averaged over 5000 disorder realization. We see that the smaller $\bar{\Delta}$, the faster the decay, which remains however power-law $C(t) \sim t^{-\beta_i}$ (dashed lines).

spread among infinitely many phonons, preventing the concurrence from stabilizing around the plateau value.

Furthermore, Fig. 7 shows that, increasing the dissipation strength ($\epsilon = 1$), the concurrence maximum becomes smaller and is reached at earlier times. However, the decay from it still follows a power-law behavior, albeit with a different exponent β_o with respect to the case of unitary evolution, as reported in Fig. 9a. This feature might be due to the specific (in particular, on-site) form of the dissipation operators in the GKSL equation. The power-law exponent β_o depends on ϵ and N , as shown in Fig. 9b, and remains finite in the thermodynamic limit. Due to the small sizes accessible when integrating the full GKSL master equation, we expect the extrapolated thermodynamic value of β_o to be underestimated (see Fig. 9b).

We note that the behavior of the concurrence is determined only by the ratio $\hbar Y_i/J_{ij}$. Remember that, in the unitary case, where the dissipation is absent, changing the typical strength of J_{ij} through the parameter R only shifts the timescale of $C(t)$, without modifying the shape of the curve (see Sec. III B 2 and Fig. 4b). Hence, in this Section, we employ the artificial parameter ϵ to investigate the behavior of pairwise entanglement exploring different regions of the phase diagram (Fig. 2) by (effectively) changing the ratio $\hbar Y_i/J_{ij}$.

Complementary to the concurrence is the half-system entanglement entropy (HSEE) $S_E(t)$, as defined in Sec. IV. Its behavior for various N and ϵ is shown in Fig. 10. As in the unitary case, HSEE starts to increase roughly when $C(t)$ reaches its maximum, i.e. as TLSs start to evolve coherently. It keeps increasing at larger times when entanglement spreads inside the system. From the data at $\epsilon = 10^{-6}$, it can be seen that the entanglement spreading takes place in two steps: first, the TLSs

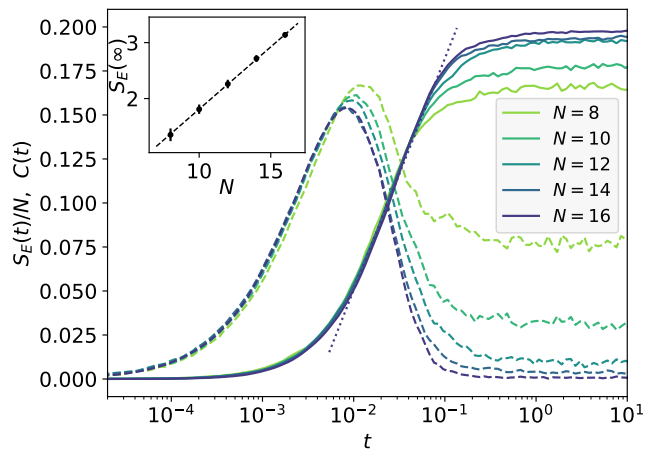


FIG. 6. Unitary evolution: entanglement entropy per unit volume $S_E(t)/N$, as defined in the main text, for various system sizes (solid lines). We set $\bar{\Delta} = 0.1$, $R = 10^3$, and averaged over 1000 disorder realization. The average concurrences $C(t)$ (Eq. (13)) are shown as dashed lines for comparison. We see that the concurrence reaches a maximum at short times, as nearby TLSs start to evolve coherently. Then, it starts to decay because the entanglement becomes many-body, as shown by the increase in the HSEE. In this regime, the growth of the HSEE is compatible with $\log(t)$: the dotted line is a fit for $N = 16$. *Inset*: The HSEE saturates to a volume law, as expected for an MBL system: the phase of each spin depends on all the others. The error bars are computed from the statistical fluctuations of the plateau values.

become entangled one with another and $S_E(t)$ reaches the plateau found with unitary dynamics ($\epsilon = 0$); then, HSEE increases further due to the dissipative term in the Lindbladian (12). Indeed, for $\epsilon \neq 0$ the TLSs entangle also with the thermal bath.

VI. CONCLUSIONS

In this article, we have investigated the well-known TLS model for glasses at low temperatures with a completely novel approach. We studied the quantum dynamics of tunnelling two-level systems coupled to phonons. Within the framework of the GKSL master equation, and by means of a weak-coupling approximation, we computed the phonon-mediated interactions among TLSs and the dissipation rates. We found that, as a consequence of disorder, the Hamiltonian responsible for the unitary part of the TLS dynamics, and accounting for TLS-TLS interactions, is completely expressed in terms of local integrals of motion, and is thus many-body localized. Even though it differs from the effective l-bit Hamiltonian of standard MBL systems because of a power-law decay of interactions, we numerically verified that the behavior of commonly considered dynamical observables, like entanglement, remains unchanged. However, the presence of dissipative terms in the GKSL equation,

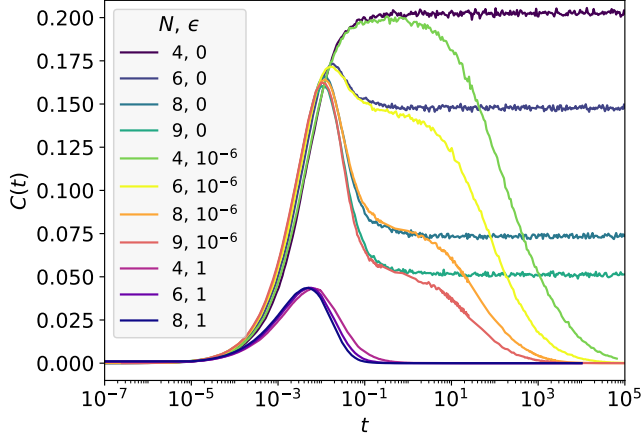


FIG. 7. $C(t)$, as defined in Eq. (13), for $\epsilon = 0, 10^{-6}, 1$, and different values of N . We see that the presence of the dissipative term in the GKSL master equation (12) decreases the concurrence maximum and moves it at earlier times. We set $\bar{\Delta} = 0.1$, $R = 10^3$, and averaged over at least 1000 disorder realizations.

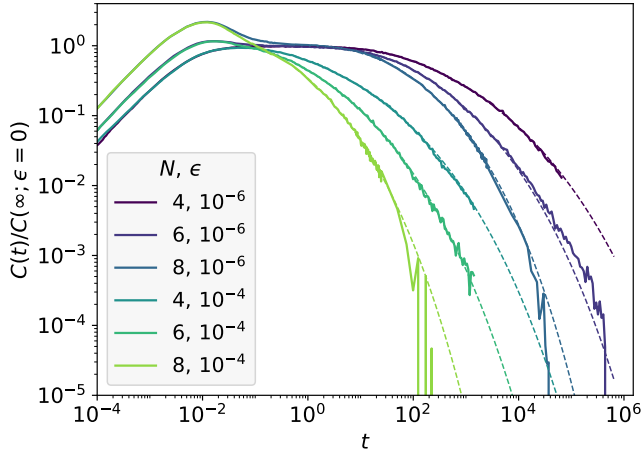


FIG. 8. Stretched-exponential fit of the concurrence for $\epsilon = 10^{-6}, 10^{-4}$, normalized to the plateau reached at $\epsilon = 0$: $C(t; \epsilon)/C(\infty; \epsilon = 0)$. Using as fitting function $\alpha \exp\{-\left(\frac{t+t_0}{\tau}\right)^\delta\}$, we obtained $\delta \simeq 0.2$ and $\tau = O(1)$. The plot shows the results for $\bar{\Delta} = 0.1$, $R = 10^3$, averaged over at least 1000 disorder realizations.

that are induced by real interactions between TLSs and phonons, destroys MBL and drives the system to thermal equilibrium at long times.

The competition between TLS-TLS interactions and dissipation determines the presence of two distinct regions in the dynamical phase diagram of the model: when interactions are stronger than dissipation, the system dynamics presents a transient *bona fide* MBL region; in the opposite case, the system quickly thermalizes. We explored the dynamical phase diagram of the model, by tuning interaction and dissipation strengths. We found numerically that, in the bulk of the MBL region, the

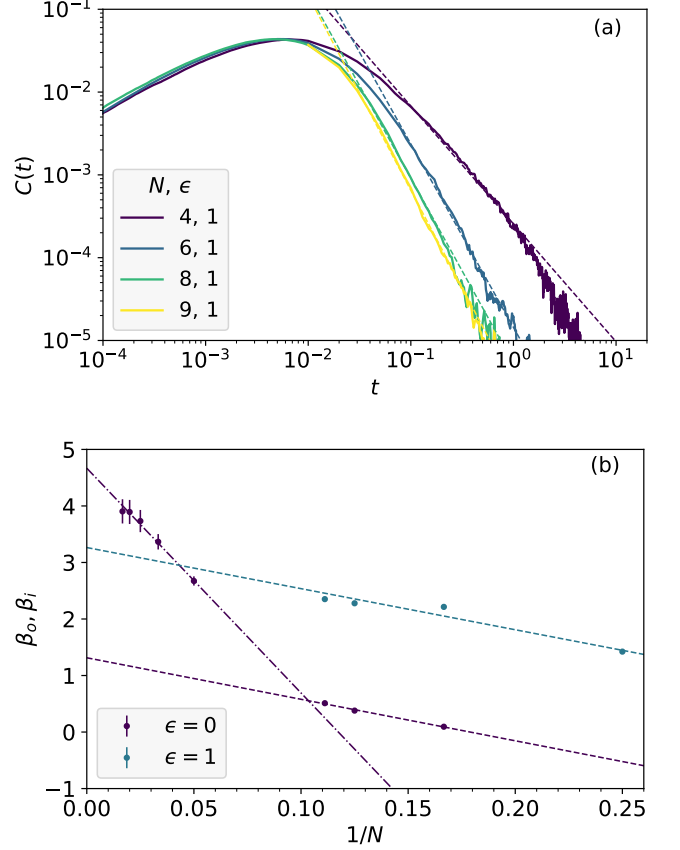


FIG. 9. (a) Power-law fit of $C(t)$ at large times for $\epsilon = 1$. (b) Power-law exponents β_i ($\epsilon = 0$; data from Fig. 3) and β_o ($\epsilon = 1$) as a function of $1/N$. We see that the concurrence decays faster as ϵ increases (dashed lines). However, our data can capture the behavior of $C(t)$ in the presence of dissipation only at small N , i.e. in the pre-asymptotic region. We expect the large N behavior to give a larger exponent β_o , as it happens for β_i (dashed-dotted line). We set $\bar{\Delta} = 0.1$, $R = 10^3$, and averaged over at least 5000 disorder realizations. The errors are computed by using the statistical uncertainties of the concurrence values.

dynamics of entanglement presents clear signatures of MBL physics, in particular in the power-law decay of the average concurrence. More surprisingly, we also observed that, for dissipation strengths not too large with respect to interactions, the dynamics of the entanglement remains unchanged.

These findings suggest that the signatures of many-body localization might be experimentally accessible, for instance using ultra-fast laser probes, in real glassy samples. Considering the typical disorder distribution parameters encompassed in the literature, it seems that real materials sit in the bulk of the transient MBL region of the phase diagram. Hence, the dynamics we have depicted in this paper should be robust from material to material and against the uncertainty in the characterization of the disorder distributions. Therefore

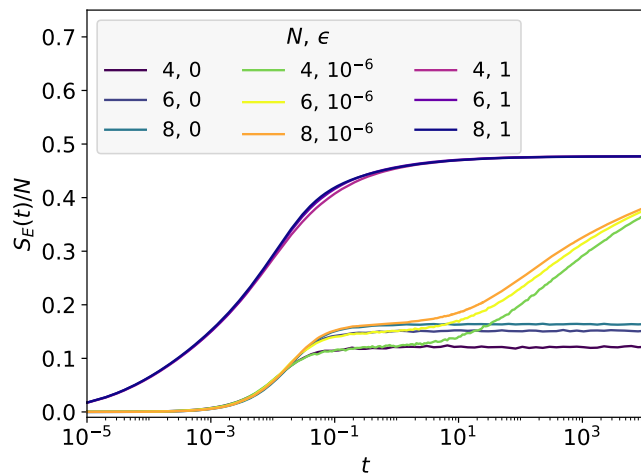


FIG. 10. Half-system entanglement entropy $S_E(t)$, as defined in Sec. IV, per number of TLSs for various N and ϵ . The plot shows the results for $\bar{\Delta} = 0.1$ and $R = 10^3$, averaged over at least 1000 disorder realizations. For $\epsilon = 10^{-6}$, we see that the entanglement spreading takes place in two steps: first, the TLSs become entangled with other TLSs and $S_E(t)/N$ reaches the plateau found in the case of unitary dynamics ($\epsilon = 0$); then, HSEE grows further due to the spread of the entanglement among TLSs and phonons. For $\epsilon = 1$, $S_E(t)/N$ is almost independent of N , indicating a volume law.

we expect it to be experimentally observable in real glassy materials at ultra-low temperatures.

We are indebted to M. Fabrizio and T. Maimbourg for valuable discussions and the careful reading of the manuscript. We are very grateful to R. Fazio, G. Giudici, S. Pappalardi, A. Russomanno, and M. Seclì for useful discussions. A.S. is also indebted to A. Leggett and G. Parisi, who have (independently) suggested that MBL signatures may be found in the physics of TLSs at low temperatures. This work is within the activities of the TQT Institute in Trieste.

-
- [1] J. M. Deutsch, Quantum statistical mechanics in a closed system, *Phys. Rev. A* **43**, 2046 (1991).
- [2] M. Srednicki, Chaos and quantum thermalization, *Phys. Rev. E* **50**, 888 (1994).
- [3] L. D'Alessio, Y. Kafri, A. Polkovnikov, and M. Rigol, From quantum chaos and eigenstate thermalization to statistical mechanics and thermodynamics, *Adv. Phys.* **65**, 239 (2016).
- [4] M. Rigol and M. Srednicki, Alternatives to eigenstate thermalization, *Phys. Rev. Lett.* **108**, 110601 (2012).
- [5] I. V. Gornyi, A. D. Mirlin, and D. G. Polyakov, Interacting electrons in disordered wires: Anderson localization and low- t transport, *Phys. Rev. Lett.* **95**, 206603 (2005).
- [6] D. M. Basko, I. L. Aleiner, and B. L. Altshuler, Metal-insulator transition in a weakly interacting many-electron system with localized single-particle states, *Ann. Phys.* **321**, 1126 (2006).
- [7] A. D. Luca and A. Scardicchio, Ergodicity breaking in a model showing many-body localization, *Europhys. Lett.* **101**, 37003 (2013).
- [8] D. A. Huse, R. Nandkishore, and V. Oganesyan, Phenomenology of fully many-body-localized systems, *Phys. Rev. B* **90**, 174202 (2014).
- [9] D. J. Luitz, N. Laflorencie, and F. Alet, Many-body localization edge in the random-field heisenberg chain, *Phys. Rev. B* **91**, 081103 (2015).
- [10] R. Nandkishore and D. A. Huse, Many-Body Localization and Thermalization in Quantum Statistical Mechanics, *Annu. Rev. Condens. Matter Phys.* **6**, 15 (2015).
- [11] D. A. Abanin and Z. Papić, Recent progress in many-body localization, *Ann. Phys.* **529**, 1700169 (2017).
- [12] D. A. Abanin, W. De Roeck, and F. Huveneers, Theory of many-body localization in periodically driven systems, *Ann. Phys.* **372**, 1 (2016).
- [13] J. Zhang, P. Hess, A. Kyprianidis, P. Becker, A. Lee, J. Smith, G. Pagano, I.-D. Potirniche, A. C. Potter, A. Vishwanath, *et al.*, Observation of a discrete time crystal, *Nature* **543**, 217 (2017).
- [14] K. Sacha and J. Zakrzewski, Time crystals: a review, *Rep. Progr. Phys.* **81**, 016401 (2017).
- [15] M. Schiulaz and M. Müller, Ideal quantum glass transitions: Many-body localization without quenched disorder, *AIP Conf. Proc.* **1610**, 11 (2014).
- [16] Z. Papić, E. M. Stoudenmire, and D. A. Abanin, Many-body localization in disorder-free systems: The importance of finite-size constraints, *Ann. Phys.* **362**, 714 (2015).
- [17] M. Pino, L. B. Ioffe, and B. L. Altshuler, Nonergodic metallic and insulating phases of josephson junction chains, *Proc. Natl. Acad. Sci. U.S.A.* **113**, 536 (2015).
- [18] N. Y. Yao, C. R. Laumann, J. I. Cirac, M. D. Lukin, and J. E. Moore, Quasi-many-body localization in translation-invariant systems, *Phys. Rev. Lett.* **117**, 240601 (2016).
- [19] R. M. Nandkishore and S. L. Sondhi, Many-body localization with long-range interactions, *Phys. Rev. X* **7**, 041021 (2017).
- [20] M. Brenes, M. Dalmonte, M. Heyl, and A. Scardicchio, Many-body localization dynamics from gauge invariance, *Phys. Rev. Lett.* **120**, 030601 (2018).
- [21] M. Schulz, C. A. Hooley, R. Moessner, and F. Pollmann, Stark many-body localization, *Phys. Rev. Lett.*

- 122**, 040606 (2019).
- [22] E. van Nieuwenburg, Y. Baum, and G. Refael, From Bloch oscillations to many-body localization in clean interacting systems, *Proc. Natl. Acad. Sci. U.S.A.* **116**, 9269 (2019).
- [23] G. Giudici, F. M. Surace, J. E. Ebot, A. Scardicchio, and M. Dalmonte, Breakdown of ergodicity in disordered $u(1)$ lattice gauge theories, *Phys. Rev. Res.* **2**, 032034 (2020).
- [24] R. C. Zeller and R. O. Pohl, Thermal conductivity and specific heat of noncrystalline solids, *Phys. Rev. B* **4**, 2029 (1971).
- [25] W. A. Phillips, Two-level states in glasses, *Rep. Progr. Phys.* **50**, 1657 (1987).
- [26] P. W. Anderson, B. I. Halperin, and C. M. Varma, Anomalous low-temperature thermal properties of glasses and spin glasses, *Phil. Mag.* **25**, 1 (1972).
- [27] W. Phillips, Tunneling states in amorphous solids, *J. Low Temp. Phys.* **7**, 351 (1972).
- [28] P. Esquinazi, *Tunneling systems in amorphous and crystalline solids* (Springer Science, 2013).
- [29] A. J. Leggett and C. C. Yu, Low temperature properties of amorphous materials: Through a glass darkly, *Comments Condens. Matter Phys.* **14**, 231 (1988).
- [30] A. J. Leggett, Amorphous materials at low temperatures: why are they so similar?, *Physica B* **169**, 322 (1991).
- [31] A. J. Leggett and D. C. Vural, “Tunneling two-level systems” model of the low-temperature properties of glasses: Are “smoking-gun” tests possible?, *J. Phys. Chem. B* **117**, 12966 (2013).
- [32] W. Arnold and S. Hunklinger, Experimental evidence for the direct interaction between two-level systems in glasses at very low temperatures, *Solid State Comm.* **17**, 883 (1975).
- [33] C. Enss and S. Hunklinger, Incoherent tunneling in glasses at very low temperatures, *Phys. Rev. Lett.* **79**, 2831 (1997).
- [34] P. Strehlow, C. Enss, and S. Hunklinger, Evidence for a phase transition in glasses at very low temperature: A macroscopic quantum state of tunneling systems?, *Phys. Rev. Lett.* **80**, 5361 (1998).
- [35] A.-M. Boiron, P. Tamarat, B. Lounis, R. Brown, and M. Orrit, Are the spectral trails of single molecules consistent with the standard two-level system model of glasses at low temperatures?, *Chem. Phys.* **247**, 119 (1999).
- [36] J. Classen, T. Burkert, C. Enss, and S. Hunklinger, Anomalous frequency dependence of the internal friction of vitreous silica, *Phys. Rev. Lett.* **84**, 2176 (2000).
- [37] J. Lisenfeld, G. J. Grabovskij, C. Müller, J. H. Cole, G. Weiss, and A. V. Ustinov, Observation of directly interacting coherent two-level systems in an amorphous material, *Nature Comm.* **6**, 6182 (2015).
- [38] A recent work[62] considers instead the situation in which the phonons modes are localized.
- [39] S. Hill and W. K. Wootters, Entanglement of a pair of quantum bits, *Phys. Rev. Lett.* **78**, 5022 (1997).
- [40] W. K. Wootters, Entanglement of formation of an arbitrary state of two qubits, *Phys. Rev. Lett.* **80**, 2245 (1998).
- [41] L. Amico, R. Fazio, A. Osterloh, and V. Vedral, Entanglement in many-body systems, *Rev. Mod. Phys.* **80**, 517 (2008).
- [42] J. Joffrin and A. Levelut, Virtual phonon exchange in glasses, *J. Phys.* **36**, 811 (1975).
- [43] K. Kassner and R. Silbey, Interactions of two-level systems in glasses, *J. Phys. Condens. Matter* **1**, 4599 (1989).
- [44] H. M. Carruzzo and C. C. Yu, Why phonon scattering in glasses is universally small at low temperatures, *Phys. Rev. Lett.* **124**, 075902 (2020).
- [45] B. Ruzicka, T. Scopigno, S. Caponi, A. Fontana, O. Pilla, P. Giura, G. Monaco, E. Pontecorvo, G. Ruocco, and F. Sette, Evidence of anomalous dispersion of the generalized sound velocity in glasses, *Phys. Rev. B* **69**, 100201 (2004).
- [46] Isotropy is due to structural disorder and holds up to short scales. A different dispersion is encountered in *ultra-stable vapor-deposited glasses*, which are essentially two-dimensional [63].
- [47] J. F. Berret and M. Meißner, How universal are the low temperature acoustic properties of glasses?, *Z. Phys. B* **70**, 65 (1988).
- [48] S. Hunklinger and A. Raychaudhuri, Chapter 3: Thermal and elastic anomalies in glasses at low temperatures (Elsevier, 1986) pp. 265–344.
- [49] H.-P. Breuer and F. Petruccione, *The Theory of Open Quantum Systems* (Oxford University Press, Oxford, 2007) p. 656.
- [50] T. E. O’Brien, D. A. Abanin, G. Vidal, and Z. Papić, Explicit construction of local conserved operators in disordered many-body systems, *Phys. Rev. B* **94**, 144208 (2016).
- [51] V. Ros, M. Müller, and A. Scardicchio, Integrals of motion in the many-body localized phase, *Nucl. Phys. B* **891**, 420 (2015).
- [52] J. Z. Imbrie, On Many-Body Localization for Quantum Spin Chains, *J. Stat. Phys.* **163**, 998 (2016).
- [53] J. Z. Imbrie, V. Ros, and A. Scardicchio, Local integrals of motion in many-body localized systems, *Ann. Phys.* **529**, 1600278 (2017).
- [54] S. Gopalakrishnan and S. Parameswaran, Dynamics and transport at the threshold of many-body localization, *Physics Reports* **862**, 1 (2020).
- [55] A. Burin and Y. Kagan, Low-energy collective excitations in glasses. new relaxation mechanism for ultralow temperatures, *J. Exp. Theor. Phys.* **80**, 633 (1994).
- [56] A. L. Burin, L. A. Maksimov, and I. Y. Polishchuk, The dephasing rate in glasses at ultra low temperatures, *Czech. J. Phys.* **46**, 2271 (1996).
- [57] O. Asban, A. Amir, Y. Imry, and M. Schechter, Effect of interactions and disorder on the relaxation of two-level systems in amorphous solids, *Phys. Rev. B* **95**, 144207 (2017).
- [58] F. Iemini, A. Russomanno, D. Rossini, A. Scardicchio, and R. Fazio, Signatures of many-body localization in the dynamics of two-site entanglement, *Phys. Rev. B* **94**, 214206 (2016).
- [59] M. Serbyn, Z. Papić, and D. A. Abanin, Quantum quenches in the many-body localized phase, *Phys. Rev. B* **90**, 174302 (2014).
- [60] M. Žnidarič, Entanglement in a dephasing model and many-body localization, *Phys. Rev. B* **97**, 214202 (2018).
- [61] M. Serbyn, Z. Papić, and D. A. Abanin, Universal slow growth of entanglement in interacting strongly disordered systems, *Phys. Rev. Lett.* **110**, 260601 (2013).
- [62] T. Maimbourg, D. M. Basko, M. Holzmann, and A. Rosso, Bath-induced zeno localization in driven many-body quantum systems, arXiv:2009.11784 (2020).
- [63] M. D. Ediger, Perspective: Highly stable vapor-deposited

glasses, J. Chem. Phys. **147**, 210901 (2017).

- [64] N. Y. Yao, C. R. Laumann, S. Gopalakrishnan, M. Knap, M. Müller, E. A. Demler, and M. D. Lukin, Many-body localization in dipolar systems, Phys. Rev. Lett. **113**, 243002 (2014).
- [65] A. L. Burin, Many-body delocalization in a strongly disordered system with long-range interactions: Finite-size scaling, Phys. Rev. B **91**, 094202 (2015).
- [66] X. Deng, A. L. Burin, and I. M. Khaymovich, Anisotropy-mediated reentrant localization, arXiv:2002.00013 (2020).
- [67] S. Lloyd and H. Pagels, Complexity as thermodynamic depth, Ann. Phys. **188**, 186 (1988).
- [68] D. N. Page, Average entropy of a subsystem, Phys. Rev. Lett. **71**, 1291 (1993).

Appendix A: Derivation of the GKSL equation

To provide a self-contained study, we review, here, the main steps leading to the GKSL master equation. The derivation can be found in more detail in many books [49].

Consider a Hamiltonian of the form

$$H_T = H_{TLS} \otimes \text{Id}_B + \text{Id}_{TLS} \otimes H_B + \gamma H_{int}$$

with $\gamma \ll 1$, where T stands for “total”, and B for “bath”. The interaction Hamiltonian is of the form

$$H_{int} = \sum_i S_i \otimes E_i,$$

with S_i acting on the TLSs and E_i on the bath only.

The time evolution of the density matrix is governed by the von Neumann equation:

$$\partial_t \rho_T = -\frac{i}{\hbar} [H_T, \rho_T].$$

To account for the interaction in perturbation theory, we switch to the interaction picture: for any operator O in the Schrödinger picture, one has $\hat{O}(t)$ in the interaction picture defined as

$$\hat{O}(t) = e^{iH_0 t/\hbar} O e^{-iH_0 t/\hbar}$$

where $H_0 := H_{TLS} + H_B$. The von Neumann equation reads

$$\partial_t \hat{\rho}_T(t) = -\frac{i\gamma}{\hbar} [\hat{H}_{int}(t), \hat{\rho}_T(t)],$$

and the corresponding integral form is

$$\hat{\rho}_T(t) = \hat{\rho}_T(0) - \frac{i\gamma}{\hbar} \int_0^t ds [\hat{H}_{int}(s), \hat{\rho}_T(s)].$$

Iterating once:

$$\begin{aligned} \partial_t \hat{\rho}_T(t) = & -\frac{i\gamma}{\hbar} [\hat{H}_{int}(t), \hat{\rho}_T(0)] \\ & - \frac{\gamma^2}{\hbar^2} \int_0^t ds [\hat{H}_{int}(t), [\hat{H}_{int}(s), \hat{\rho}_T(s)]] . \end{aligned}$$

Neglecting $o(\gamma^2)$, this is equivalent to

$$\begin{aligned} \partial_t \hat{\rho}_T(t) \simeq & -\frac{i\gamma}{\hbar} [\hat{H}_{int}(t), \hat{\rho}_T(0)] \\ & - \frac{\gamma^2}{\hbar^2} \int_0^t ds [\hat{H}_{int}(t), [\hat{H}_{int}(s), \hat{\rho}_T(s)]] , \end{aligned} \quad (\text{A1})$$

where the unknown $\hat{\rho}_T$ appears only at time t .

Now, the environment can be traced out. Calling the reduced density matrix $\text{Tr}_B \hat{\rho}_T := \hat{\rho}$, we get

$$\begin{aligned} \partial_t \hat{\rho}(t) = & \text{Tr}_B [\partial_t \hat{\rho}_T(t)] \\ = & -\frac{i\gamma}{\hbar} \text{Tr}_B [\hat{H}_{int}(t), \hat{\rho}_T(0)] \\ & - \frac{\gamma^2}{\hbar^2} \int_0^t ds \text{Tr}_B [\hat{H}_{int}(t), [\hat{H}_{int}(s), \hat{\rho}_T(s)]] . \end{aligned} \quad (\text{A2})$$

At this point, we make the following assumptions:

- The initial density matrix is factorized:

$$\rho_T(0) = \rho(0) \otimes \rho_B(0). \quad (\text{A3})$$

- The initial bath density matrix is thermal at inverse temperature $\beta = 1/k_B T$:

$$\rho_B(0) = \rho_B^T := \frac{e^{-\beta H_B}}{Z}. \quad (\text{A4})$$

Moreover, we also employ the following approximation:

$$\hat{\rho}_T(t) = \hat{\rho}(t) \otimes \rho_B^T. \quad (\text{A5})$$

This means that the influence of the TLSs on the phonon bath is negligible at all times.

Using $\text{Tr}_B(\rho_B E_i) = 0$ (every constant shift can be reabsorbed in H_{TLS}), Eq. (A2) becomes

$$\begin{aligned} \partial_t \hat{\rho}(t) = & -\frac{\gamma^2}{\hbar^2} \int_0^t ds \text{Tr}_B [\hat{H}_{int}(t), \\ & [\hat{H}_{int}(s), \hat{\rho}(t) \otimes \rho_B^T]]. \end{aligned}$$

This equation is *non-Markovian*: it depends on the initial condition at $t = 0$ for $\rho(t)$. We can get a *Markovian* equation by extending the range of time integration to the infinitely far past:

$$\begin{aligned} \partial_t \hat{\rho}(t) = & -\frac{\gamma^2}{\hbar^2} \int_0^\infty ds \text{Tr}_B [\hat{H}_{int}(t), \\ & [\hat{H}_{int}(t-s), \hat{\rho}(t) \otimes \rho_B^T]]. \end{aligned} \quad (\text{A6})$$

This is known as *Redfield equation*. Unfortunately, in general this equation does not preserve the positivity of the density matrix.

At this point it is convenient to find the explicit expression of $\hat{H}_{int}(t)$. Therefore, we decompose (note that in the absence of hats the picture is Schrödinger's!)

$$S_i = \sum_{\nu \in \mathcal{F}_i} c_i^\nu S_i^\nu, \quad (\text{A7})$$

S_i^ν being s.t. $[H_{TLS}, S_i^\nu] = -\hbar\nu S_i^\nu$. The coefficients c_i^ν could be reabsorbed into the definition of the operators S_i , but in this way the notation matches with the main text. Also, we denote as \mathcal{F}_i the set of all the eigenfrequencies of S_i . It follows

$$\hat{H}_{int}(t) = \sum_j \sum_{\nu \in \mathcal{F}_j} c_j^\nu e^{-i\nu t} S_j^\nu \otimes \hat{E}_j(t).$$

Plugging this equation into the triple commutator and regrouping terms yields

$$\begin{aligned} \partial_t \hat{\rho}(t) = \sum_{ij} \sum_{\nu \in \mathcal{F}_j} \sum_{\nu' \in \mathcal{F}_i} \left\{ c_i^{\nu'} c_j^\nu e^{i(\nu' - \nu)t} \right. \\ \left. \times \Gamma_{ij}^\nu [S_j^\nu \hat{\rho}(t), S_i^{\nu'\dagger}] + \text{h.c.} \right\} \end{aligned}$$

with

$$\Gamma_{ij}^\nu := \frac{\gamma^2}{\hbar^2} \int_0^\infty ds e^{i\nu s} \text{Tr}_B \left[\rho_B^T \hat{E}_i^\dagger(t) \hat{E}_j(t-s) \right]. \quad (\text{A8})$$

To proceed further, and recover the positivity of $\rho(t)$, we perform the so-called *rotating-wave approximation*, i.e. we retain only the resonant $\nu = \nu'$ terms:

$$\begin{aligned} \partial_t \hat{\rho}(t) = \sum_{ij} \sum_{\nu \in \mathcal{F}_i \cap \mathcal{F}_j} c_i^{\nu*} c_j^\nu \left\{ \Gamma_{ij}^\nu [S_j^\nu \hat{\rho}(t), S_i^{\nu\dagger}] \right. \\ \left. + \Gamma_{ji}^{\nu*} [S_j^\nu, \hat{\rho}(t) S_i^{\nu\dagger}] \right\}. \quad (\text{A9}) \end{aligned}$$

Finally, we transform everything back to the Schrödinger picture:

$$\begin{aligned} \partial_t \rho(t) = -\frac{i}{\hbar} [H_{TLS} + H_{LS}, \rho(t)] \\ + \sum_{ij} \sum_{\nu \in \mathcal{F}_i \cap \mathcal{F}_j} Y_{ij}^\nu \left[S_j^\nu \rho(t) S_i^{\nu\dagger} - \frac{1}{2} \{ S_i^{\nu\dagger} S_j^\nu, \rho(t) \} \right] \quad (\text{A10}) \end{aligned}$$

where H_{LS} is the *Lamb-Stark shift* Hamiltonian

$$H_{LS} := \sum_{ij} \sum_{\nu \in \mathcal{F}_i \cap \mathcal{F}_j} J_{ij}^\nu S_i^{\nu\dagger} S_j^\nu \quad (\text{A11})$$

and

$$Y_{ij}^\nu := c_i^{\nu*} c_j^\nu \Upsilon_{ij}^\nu := c_i^{\nu*} c_j^\nu (\Gamma_{ij}^\nu + \Gamma_{ji}^{\nu*}), \quad (\text{A12})$$

$$J_{ij}^\nu := c_i^{\nu*} c_j^\nu \hbar \Pi_{ij}^\nu := c_i^{\nu*} c_j^\nu \frac{\hbar}{2i} (\Gamma_{ij}^\nu - \Gamma_{ji}^{\nu*}). \quad (\text{A13})$$

The celebrated *Gorini-Kossakowski-Sudarshan-Lindblad equation* is obtained upon diagonalizing the ij indices:

$$\begin{aligned} \partial_t \rho(t) = -\frac{i}{\hbar} [H_{TLS} + H_{LS}, \rho(t)] \\ + \sum_{\kappa} \sum_{\nu \in \mathcal{F}_\kappa} \left[L_\kappa^\nu \rho(t) L_\kappa^{\nu\dagger} - \frac{1}{2} \{ L_\kappa^{\nu\dagger} L_\kappa^\nu, \rho(t) \} \right] \quad (\text{A14}) \end{aligned}$$

In the main text we will stick however to Eqs. (A10)–(A13).

Appendix B: The thermalization rates

The decoherence rates Υ_{ij}^ν can be computed from Eq. (A12) and Eq. (6). Noting that $\mathcal{F}_i \cap \mathcal{F}_j = \{0\}$ with high probability if $i \neq j$, and since $\Upsilon_{ij}^0 = 0$ (as will become evident later on), the main contribution to the relaxation comes from Υ_{ii}^\pm .

Hence, we find

$$\Upsilon_{ii}^\nu = \frac{\pi \gamma_i^2}{4\rho} \sum_{abcd} D_i^{ab} D_i^{cd} \sum_\alpha \int \frac{d^3 q}{(2\pi)^3} \frac{1}{\hbar \omega_k} (q^a \hat{e}_k^b + q^b \hat{e}_k^a) (q^c \hat{e}_k^d + q^d \hat{e}_k^c) [(f_T(\hbar \omega_k) + 1) \delta(\nu - \omega_k) + f_T(\hbar \omega_k) \delta(\nu + \omega_k)].$$

The computation of Υ_{ii}^ν is simplified by splitting the polarization sum into transverse and longitudinal modes. For the latter $\hat{\mathbf{e}}_{\mathbf{q},L} = \hat{\mathbf{q}}$ and $\hbar \omega_{\mathbf{q},L} = v_L |\mathbf{q}|$. It follows that the angular integral can be performed rather easily:

$$\sum_{abcd} D_i^{ab} D_i^{cd} \int d\Omega (\hat{q}^a \hat{q}^b \hat{q}^c \hat{q}^d + (a \leftrightarrow c; b \leftrightarrow d)) = \frac{16\pi}{15} \sum_{ab} (D_i^{aa} D_i^{bb} + D_i^{ab} D_i^{ab} + D_i^{ab} D_i^{ba}) =: \frac{16\pi}{15} \langle\langle D_i D_i \rangle\rangle_{\Upsilon,L}.$$

Then the longitudinal contribution to Υ_{ii}^ν is

$$[\Upsilon_{ii}^\nu]_L = \frac{\gamma_i^2 \langle\langle D_i D_i \rangle\rangle_{\Upsilon,L}}{30\pi \rho \hbar} \int_0^\infty dq q^4 \frac{1}{v_L q} [(f_T(\hbar v_L q) + 1) \delta(\nu - v_L q) + f_T(\hbar v_L q) \delta(\nu + v_L q)].$$

One has to consider separately the cases for the different $\nu \in \mathcal{F}_i$. If $\nu = \nu_{i,0} = 0$, then $[\Upsilon_{ii}^0]_L = 0$ (the phonons have zero density of states at zero frequency). Each one of the other two cases, $\nu = \nu_{i,\pm}$, selects just one of the two delta

functions. Calling $\nu_i := |\nu_{i,\pm}|$, we arrive at

$$[\Upsilon_{ii}^+]_L = \frac{\gamma_i^2 \langle\langle D_i D_i \rangle\rangle_{\Upsilon,L} (\hbar\nu_i)^3}{30\pi\rho\hbar^4 v_L^5} (f_T(\hbar\nu_i) + 1), \quad [\Upsilon_{ii}^-]_L = \frac{\gamma_i^2 \langle\langle D_i D_i \rangle\rangle_{\Upsilon,L} (\hbar\nu_i)^3}{30\pi\rho\hbar^4 v_L^5} f_T(\hbar\nu_i).$$

For the transverse modes, instead, it holds

$$\sum_{\alpha \text{ trans.}} \hat{e}_{\mathbf{q},\alpha}^a \hat{e}_{\mathbf{q},\alpha}^b = \delta^{ab} - \hat{q}^a \hat{q}^b, \quad (\text{B1})$$

and the angular integral gives

$$\begin{aligned} \sum_{abcd} D_i^{ab} D_i^{cd} \int d\Omega (\hat{q}^a \hat{q}^c (\delta^{bd} - \hat{q}^b \hat{q}^d) + (a \leftrightarrow c; b \leftrightarrow d)) \\ = \frac{4\pi}{15} \sum_{ab} (D_i^{ab} D_i^{ab} - 4D_i^{aa} D_i^{bb} - 4D_i^{ab} D_i^{ba}) =: \frac{16\pi}{15} \langle\langle D_i D_i \rangle\rangle_{\Upsilon,T}. \end{aligned}$$

As for the longitudinal modes, each $\nu \in \mathcal{F}_i$ has to be treated separately. We find $[\Upsilon_{ii}^0]_T = 0$ and

$$\begin{aligned} [\Upsilon_{ii}^+]_T &= \frac{\gamma_i^2 \langle\langle D_i D_i \rangle\rangle_{\Upsilon,T} (\hbar\nu_i)^3}{30\pi\rho\hbar^4 v_T^5} (f_T(\hbar\nu_i) + 1), \\ [\Upsilon_{ii}^-]_T &= \frac{\gamma_i^2 \langle\langle D_i D_i \rangle\rangle_{\Upsilon,T} (\hbar\nu_i)^3}{30\pi\rho\hbar^4 v_T^5} f_T(\hbar\nu_i). \end{aligned}$$

Appendix C: The Lamb-Stark shift Hamiltonian

The Lamb-Stark shift Hamiltonian is expressed in terms of Π_{ij}^ν , defined in Eq. (A13). From Eq. (6) we find

$$\begin{aligned} \Pi_{ij}^\nu &= \frac{\gamma_i \gamma_j}{8\rho} \sum_{abcd} D_i^{ab} D_j^{cd} \sum_{\alpha} \text{PV} \int \frac{d^3q}{(2\pi)^3} \frac{1}{\hbar\omega_k} (q^a \hat{e}_k^b + q^b \hat{e}_k^a) (q^c \hat{e}_k^d + q^d \hat{e}_k^c) \\ &\quad \times \left[(f_T(\hbar\omega_k) + 1) \frac{1}{\nu - \omega_k} e^{i\mathbf{q}\cdot(\mathbf{r}_i - \mathbf{r}_j)} + f_T(\hbar\omega_k) \frac{1}{\nu + \omega_k} e^{-i\mathbf{q}\cdot(\mathbf{r}_i - \mathbf{r}_j)} \right]. \quad (\text{C1}) \end{aligned}$$

We can proceed as in the previous Section: we split the different polarization contributions, then evaluate the angular integrals, and, finally, the $|\mathbf{q}|$ integral. The angular integrals will be of two types: either they contain four unit \mathbf{q} -vectors (these appear both for longitudinal and transverse polarizations) or they contain two unit \mathbf{q} -vectors (for transverse polarizations only). This follows upon using Eq. (B1). We put the $\hat{\mathbf{z}}$ -axis parallel to $(\mathbf{r}_i - \mathbf{r}_j)$ and define

$$\begin{aligned} I_{abcd}(\zeta) &:= \frac{1}{4\pi} \int d\Omega \hat{q}^a \hat{q}^b \hat{q}^c \hat{q}^d e^{i\zeta \cos \theta}, \\ I_{ab}(\zeta) &:= \frac{1}{4\pi} \int d\Omega \hat{q}^a \hat{q}^b e^{i\zeta \cos \theta}. \end{aligned}$$

Explicitly:

$$\begin{aligned} I_{xyyy}(\zeta) &= \frac{1}{3} I_{xxxx}(\zeta) = -\frac{3\zeta \cos \zeta + (\zeta^2 - 3) \sin \zeta}{\zeta^5}, \\ I_{xxzz}(\zeta) &= -\frac{\zeta(\zeta^2 - 12) \cos \zeta - (5\zeta^2 - 12) \sin \zeta}{\zeta^5}, \end{aligned}$$

$$\begin{aligned} I_{zzzz}(\zeta) &= \frac{4\zeta(\zeta^2 - 6) \cos \zeta + (\zeta^4 - 12\zeta^2 + 24) \sin \zeta}{\zeta^5}, \\ I_{xx}(\zeta) &= \frac{-\zeta \cos \zeta + \sin \zeta}{\zeta^3}, \\ I_{zz}(\zeta) &= \frac{2\zeta \cos \zeta + (\zeta^2 - 2) \sin \zeta}{\zeta^3}. \end{aligned}$$

Similar ones are obtained exchanging x and y and permuting the indices; all the others are zero. We can then parametrize

$$\begin{aligned} I_{abcd}(\zeta) &= \frac{1}{\zeta^5} \sum_{l=0}^4 C_{abcd}^l \zeta^l s_l(\zeta), \\ I_{ab}(\zeta) &= \frac{1}{\zeta^3} \sum_{l=0}^2 C_{ab}^l \zeta^l s_l(\zeta) \end{aligned}$$

where

$$s_l(\zeta) := \begin{cases} \sin \zeta & l \text{ even} \\ \cos \zeta & l \text{ odd.} \end{cases}$$

At this point, we can simplify a bit the tensorial sums. For the longitudinal mode we have

$$\begin{aligned} \sum_{abcd} D_i^{ab} D_j^{cd} (I_{abcd} + (a \leftrightarrow c; b \leftrightarrow d)) \\ = \sum_{abcd} D_i^{\{ab\}} D_j^{\{cd\}} I_{abcd} \end{aligned}$$

$D_i^{ab} + D_i^{ba}$. For the transverse modes instead

$$\begin{aligned} \sum_{abcd} D_i^{ab} D_j^{cd} (I_{ac} \delta^{bd} - I_{abcd} + (a \leftrightarrow c; b \leftrightarrow d)) \\ = \sum_{abc} D_i^{\{ac\}} D_j^{\{bc\}} I_{ab} - \sum_{abcd} D_i^{\{ab\}} D_j^{\{cd\}} I_{abcd}. \end{aligned}$$

1. Longitudinal contribution

where $\{ab\}$ stands for the symmetrized sum $D_i^{\{ab\}} :=$

The longitudinal case is clearly easier. We have, setting $\zeta := qr_{ij}$ and taking into account the parity of $s_l(\zeta)$,

$$\begin{aligned} [\Pi_{ij}^\nu]_L = \frac{\gamma_i \gamma_j}{16\pi^2 \rho \hbar v_L^2 r_{ij}^3} \sum_{l=0}^4 \left[\sum_{abcd} D_i^{\{ab\}} D_j^{\{cd\}} C_{abcd}^l \right] \\ \times \text{PV} \int_0^\infty d\zeta \zeta^{l-2} s_l(\zeta) \left[\frac{1}{e^{\beta \hbar \nu \zeta / r_{ij}} - 1} \frac{2r_{ij}\nu/v_L}{(r_{ij}\nu/v_L)^2 - \zeta^2} + \frac{1}{r_{ij}\nu/v_L - \zeta} \right]. \end{aligned}$$

We note that, because of the condition $\nu \in \mathcal{F}_i \cap \mathcal{F}_j$, essentially only the frequency $\nu = 0$ will contribute to the interaction. With this simplification, we separate the zero-point from the temperature-dependent contributions by defining

$$J_l^{\text{zp}} := \lim_{a \rightarrow 0} \text{PV} \int_0^\infty d\zeta \frac{\zeta^{l-2} s_l(\zeta)}{a - \zeta}, \quad J_l(b) := \lim_{a \rightarrow 0} \text{PV} \int_0^\infty d\zeta \frac{\zeta^{l-2} s_l(\zeta)}{e^{b\zeta} - 1} \frac{2a}{a^2 - \zeta^2}. \quad (\text{C2})$$

The limit $a \rightarrow 0$ has to be taken after the integration, since the principal value needs a two-sided limit around the singularity.

We can now compute all the integrals.

a. $l = 0, 1$. First, we note that for $l = 0$ and $l = 1$ both $J_{0,1}^{\text{zp}}$ and $J_{0,1}(b)$ are IR divergent. However, considering Eq. (C1), there cannot be infrared divergences: this suggests that the divergences compensate. To see it more explicitly, we add and subtract a term as follows:

$$\begin{aligned} J_0^{\text{zp}} &\equiv \lim_{a \rightarrow 0} \left\{ \text{PV} \int_0^\infty d\zeta \frac{\sin \zeta - \zeta}{\zeta^2(a - \zeta)} + \text{PV} \int_0^\infty d\zeta \frac{1}{\zeta(a - \zeta)} \right\}, \\ J_1^{\text{zp}} &\equiv \lim_{a \rightarrow 0} \left\{ \text{PV} \int_0^\infty d\zeta \frac{\cos \zeta - 1}{\zeta(a - \zeta)} + \text{PV} \int_0^\infty d\zeta \frac{1}{\zeta(a - \zeta)} \right\}. \end{aligned}$$

The added and subtracted term is the same for the two integrals, and it makes them convergent. Moreover, it is easy to check that $C_{abcd}^0 = -C_{abcd}^1$. This means that the divergent parts cancel exactly, and one is left with a finite result. The regularized integrals can be evaluated exactly:

$$J_0^{\text{zp}} = \frac{\pi}{4} + J_{\text{diverg}}^{\text{zp}}, \quad J_1^{\text{zp}} = \frac{\pi}{2} + J_{\text{diverg}}^{\text{zp}}.$$

The same can be done with the temperature-dependent part:

$$\begin{aligned} J_0(b) &\equiv \lim_{a \rightarrow 0} \left\{ \text{PV} \int_0^\infty d\zeta \frac{2a(\sin \zeta - \zeta)}{\zeta^2(e^{b\zeta} - 1)(a^2 - \zeta^2)} + \text{PV} \int_0^\infty d\zeta \frac{2a}{\zeta(e^{b\zeta} - 1)(a^2 - \zeta^2)} \right\}, \\ J_1(b) &\equiv \lim_{a \rightarrow 0} \left\{ \text{PV} \int_0^\infty d\zeta \frac{2a(\cos \zeta - 1)}{\zeta(e^{b\zeta} - 1)(a^2 - \zeta^2)} + \text{PV} \int_0^\infty d\zeta \frac{2a}{\zeta(e^{b\zeta} - 1)(a^2 - \zeta^2)} \right\}. \end{aligned}$$

As for the zero-point contribution, the added and subtracted term is the same for the two integrals and makes

them convergent. Since $C_{abcd}^0 = -C_{abcd}^1$, the divergent

parts cancel exactly. Moreover, since $J_l(b) \propto a$, the finite contributions given by the regularized integrals go to 0 when $a \rightarrow 0$. Hence,

$$J_0(b) = J_{\text{diverg}}(b), \quad J_1(b) = J_{\text{diverg}}(b),$$

and the temperature-dependent parts do not contribute.

b. $l = 2$. The zero-point contribution can be evaluated exactly:

$$J_2^{\text{zp}} = -\frac{\pi}{2}$$

The temperature-dependent integral is instead finite for $a \neq 0$, and goes to zero in the limit $a \rightarrow 0$.

c. $l = 3, 4$. It holds $J_{3,4}^{\text{zp}} = 0$: the limit $a \rightarrow 0$ can be taken inside the integral, which becomes conditionally convergent to 0. Also, as for $l = 2$, the temperature-

dependent integrals go to 0 with a .

d. Collecting results. From what found above, it follows

$$\begin{aligned} [\Pi_{ij}^0]_L &= -\frac{\gamma_i \gamma_j}{32\pi\rho\hbar} \frac{1}{v_L^2 r_{ij}^3} \\ &\times \sum_{abcd} D_i^{\{ab\}} D_j^{\{cd\}} \left[\frac{1}{2} C_{abcd}^0 + C_{abcd}^2 \right] \\ &=: -\frac{\gamma_i \gamma_j}{32\pi\rho\hbar} \frac{\langle\langle D_i D_j \rangle\rangle_{\Pi,L}}{v_L^2 r_{ij}^3}. \quad (\text{C3}) \end{aligned}$$

2. Transverse contribution

The transverse modes have both a term almost equal to the longitudinal one, and one involving I_{ab} :

$$\begin{aligned} [\Pi_{ij}^\nu]_T &= \frac{\gamma_i \gamma_j}{16\pi^2 \rho \hbar} \frac{1}{v_T^2 r_{ij}^3} \sum_{l=0}^2 \left[\sum_{abcd} D_i^{\{ac\}} D_j^{\{cb\}} C_{ab}^l \right] \\ &\times \text{PV} \int_0^\infty d\zeta \zeta^l s_l(\zeta) \left[\frac{1}{e^{\beta\hbar\nu_T \zeta / r_{ij}} - 1} \frac{2r_{ij}\nu / v_T}{(r_{ij}\nu / v_T)^2 - \zeta^2} + \frac{1}{r_{ij}\nu / v_T - \zeta} \right] - (\dots) \end{aligned}$$

where the omitted term is exactly equal to Eq. (C3), as long as one changes v_L to v_T . Moreover, the new term is very similar to that obtained for the longitudinal modes: one has just to shift $l \rightarrow l + 2$. The result is

$$\begin{aligned} [\Pi_{ij}^0]_T &= -\frac{\gamma_i \gamma_j}{32\pi\rho\hbar} \frac{1}{v_T^2 r_{ij}^3} \\ &\times \sum_{abcd} D_i^{\{ab\}} D_j^{\{cd\}} \left[C_{ac}^0 \delta^{bd} - \frac{1}{2} C_{abcd}^0 - C_{abcd}^2 \right] \\ &=: -\frac{\gamma_i \gamma_j}{32\pi\rho\hbar} \frac{\langle\langle D_i D_j \rangle\rangle_{\Pi,T}}{v_T^2 r_{ij}^3}. \end{aligned}$$

3. Final result

The final result for the Lamb-Stark interactions is obtained by adding the longitudinal and the transverse contributions:

$$\begin{aligned} \Pi_{ij}^0 &= [\Pi_{ij}^0]_L + [\Pi_{ij}^0]_T \\ &= -\frac{\gamma_i \gamma_j}{32\pi\rho\hbar r_{ij}^3} \left[\frac{\langle\langle D_i D_j \rangle\rangle_{\Pi,L}}{v_L^2} + \frac{\langle\langle D_i D_j \rangle\rangle_{\Pi,T}}{v_T^2} \right]. \quad (\text{C4}) \end{aligned}$$

Note that this expression has been found in a previous study [42] by means of time-independent perturbation theory.

Appendix D: Higher order effects

In the framework of the GKSL master equation, the interactions of the Lamb-Stark shift Hamiltonian have a particular structure. Because of the rotating-wave approximation, only terms that commute with the free TLS evolution can appear. It may happen, however, that some rare couples of TLS resonate and terms $\propto (S_i^+ S_j^- + \text{h.c.})$ and $\propto (S_i^+ S_j^+ + \text{h.c.})$ have to be introduced. These terms were also introduced on heuristic grounds in some previous works [28, 55, 56].

If such terms are present in the Hamiltonian, a different analysis has to be performed. The Hamiltonian becomes that of a system of dipoles, whose MBL transition has been already addressed [64–66].

Appendix E: Concurrence in a random state

Let us consider a system of N spin-1/2. A (uniformly distributed) random state is $|\psi\rangle = U|\psi_0\rangle$ with U being a Haar-random unitary, and $|\psi_0\rangle$ a reference state. Equivalently, a random state is $|\psi\rangle = \sum_{\{s\}} A_{\{s\}} |\{s\}\rangle$, with the coefficients $A_{\{s\}}$ being (uniformly) distributed over $\mathbb{C}P^{M-1}$, with $M = 2^N$.

If we compute the concurrence of two spins, say, without loss of generality, sites 1 and 2, we need to com-

pute the square roots of the eigenvalues of the matrix $R_{12} = \rho_{12}(\sigma_y \otimes \sigma_y) \rho_{12}^*(\sigma_y \otimes \sigma_y)$. The exact determination of such eigenvalues has evaded our analytical attempts, but we can give an heuristic argument that captures the

scaling with N . Consider, instead of the square roots of the eigenvalues of R_{12} , directly the eigenvalues λ_a of ρ_{12} . Classical works[67, 68] give us their probability density function:

$$p(\lambda_1, \lambda_2, \lambda_3, \lambda_4) \propto \delta\left(1 - \sum_{a=1}^4 \lambda_a\right) \prod_{a=1}^4 \lambda_a^{M-4} \prod_{a<b} (\lambda_a - \lambda_b)^2$$

with the constraint $\lambda_a > 0$, $a = 1, \dots, 4$. With hindsight, we perform the change of variables

$$\rho_{12} \equiv \frac{1}{4} \text{Id} + \frac{1}{4\sqrt{M-4}} \tau_{12}, \quad \lambda_a \equiv \frac{1}{4} + \frac{\mu_a}{4\sqrt{M-4}},$$

so that

$$\begin{aligned} p(\mu_1, \mu_2, \mu_3, \mu_4) &\propto \delta\left(\sum_{a=1}^4 \mu_a\right) \prod_{a=1}^4 \left(1 + \frac{\mu_a}{\sqrt{M-4}}\right)^{M-4} \prod_{a<b} (\mu_a - \mu_b)^2 \\ &\propto \delta\left(\sum_{a=1}^4 \mu_a\right) \exp\left[-\frac{1}{2} \sum_a \mu_a^2 + O\left(\frac{1}{\sqrt{M-4}}\right)\right] \prod_{a<b} (\mu_a - \mu_b)^2. \end{aligned}$$

We see that, at this order, we can let μ_a range from $-\infty$ to $+\infty$ if N is big enough.

At this point we note that not only the eigenvalues of τ_{12} , but every entry of the matrix is at most of order 1 because of our rescaling. This enables us to expand

$$\begin{aligned} \sqrt{R_{12}} &= \left[\frac{1}{16} \text{Id} + \frac{1}{16\sqrt{M-4}} [\tau_{12} + (\sigma_y \otimes \sigma_y) \tau_{12}^* (\sigma_y \otimes \sigma_y)] + O\left(\frac{1}{M}\right) \right]^{1/2} \\ &= \frac{1}{4} \text{Id} + \frac{1}{8\sqrt{M-4}} [\tau_{12} + (\sigma_y \otimes \sigma_y) \tau_{12}^* (\sigma_y \otimes \sigma_y)] + O\left(\frac{1}{M}\right) \end{aligned}$$

The matrix $\frac{1}{2}[\tau_{12} + (\sigma_y \otimes \sigma_y) \tau_{12}^* (\sigma_y \otimes \sigma_y)]$ is traceless and very roughly its eigenvalues will have a joint probability density function very similar to that of τ_{12} . For this reason, we can approximate the average concurrence with

$$\langle C \rangle \approx \int d\vec{\mu} p(\vec{\mu}) \max\left\{0, \frac{2\mu_1 - 1}{4\sqrt{M-4}} - \frac{1}{2}\right\},$$

where we have used the δ -function constraint and called μ_1 the largest eigenvalue. Integrating only on μ_1 , and forgetting the presence of μ_2, μ_3, μ_4 (otherwise the integration becomes rather cumbersome), we find

$$\langle C \rangle \approx \frac{e^{-(M+\sqrt{M-4})/2}}{2\sqrt{2\pi}(M-4)^{3/2}},$$

from which

$$\log_2(-\log\langle C \rangle) \approx \log(a) + bN + \dots \quad (\text{E1})$$

with $a = 1/2$ and $b = 1$. As can be seen from Figure 11, this scaling is correct, but the numerical factor a is different.

Appendix F: Integration of the GKSL master equation

The density matrix of the system can be parametrized as

$$\rho(t) = \sum_{\mu_1 \dots \mu_N} C_{\mu_1 \dots \mu_N}(t) S_1^{\mu_1} \otimes \dots \otimes S_N^{\mu_N},$$

where $S_i^{\mu_i} \in \{\text{Id}_i, S_i^+, S_i^-, S_i^0\}$. Writing explicitly the GKSL equation (see Eqs. (10) and (11) in the main text), we get

$$\begin{aligned} \partial_t \rho(t) &= \frac{i}{\hbar} \left[\frac{1}{2} \sum_i \hbar \nu_i S_i^0 - \sum_{ij} J_{ij} S_i^0 S_j^0, \rho(t) \right] \\ &+ \sum_i Y_i f_T(\hbar \nu_i) [S_i^+ \rho(t) S_i^- + S_i^- \rho(t) S_i^+ - 4\rho(t)] \\ &+ \sum_i Y_i [S_i^+ \rho(t) S_i^- + \{\rho(t), S_i^0\} - 2\rho(t)]. \end{aligned}$$

In absence of the interactions (i.e. ignoring the term $\sum_{ij} J_{ij} S_i^0 S_j^0$), the evolution can be easily computed, and

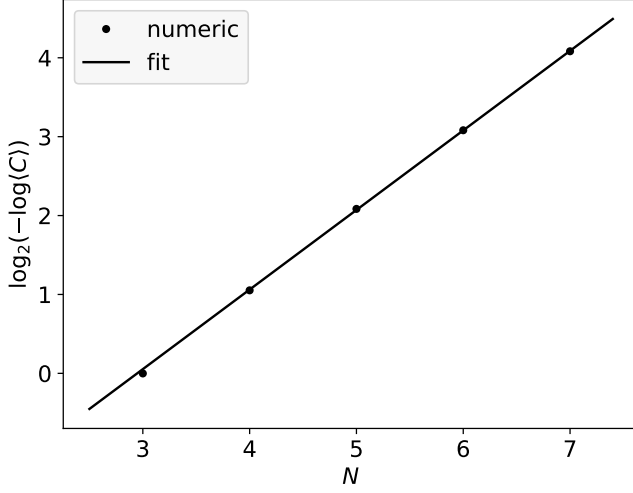


FIG. 11. The average concurrence in a random state follows the scaling $\langle C \rangle \sim e^{-a2^{bN}}$. The dots show the concurrence averaged over 10^7 randomly generated states, and over every couple of spins for each state. A linear fit is shown for comparison: $b = 1.009(6)$, but $a = 0.127(3)$, differing from $a = 1/2$ found analytically (Eq. (E1)).

the density matrix evolves as

$$\partial_t C_{\mu_1 \dots \mu_N} = \left[\sum_i \lambda_i^{\mu_i} \right] C_{\mu_1 \dots \mu_N} + \sum_i 4Y_i \delta^{\mu_i 3} C_{\mu_1 \dots 0_i \dots \mu_N},$$

where the $\delta^{\mu_i 3}$ are Kronecker deltas, the $\lambda_i^{\mu_i}$'s are given by

$$\lambda_i^3 = -4Y_i(1 + 2f_T), \quad \lambda_i^\pm = \frac{1}{2}\lambda_i^3 \pm i\nu_i,$$

and $\lambda_i^0 = 0$. When interactions are suppressed, the TLSs evolve independently one from the other and any factorized initial state will remain such at all times. One has

$$\rho(t) = \bigotimes_{i=1}^N \sum_{\mu_i} P_i^{\mu_i}(t) S_i^{\mu_i} \implies C_{\mu_1 \dots \mu_N}(t) = P_1^{\mu_1}(t) \dots P_N^{\mu_N}(t) \quad \forall t.$$

The interactions among TLSs make the evolution more complicated. Computing the commutator

$$\begin{aligned} [S_i^0 S_j^0, S_i^{\mu_i} S_j^{\mu_j}] &= S_i^0 S_i^{\mu_i} [S_j^0, S_j^{\mu_j}] + [S_i^0, S_i^{\mu_i}] S_j^{\mu_j} S_j^0 \\ &= 2 \sum_{\nu_i \nu_j} [(\delta^{\mu_i 0} \delta^{\nu_i 3} + \delta^{\mu_i 3} \delta^{\nu_i 0} + \delta^{\mu_i +} \delta^{\nu_i +} - \delta^{\mu_i -} \delta^{\nu_i -})(\delta^{\mu_j +} \delta^{\nu_j +} - \delta^{\mu_j -} \delta^{\nu_j -}) \\ &\quad + (\delta^{\mu_j 0} \delta^{\nu_j 3} + \delta^{\mu_j 3} \delta^{\nu_j 0} - \delta^{\mu_j +} \delta^{\nu_j +} + \delta^{\mu_j -} \delta^{\nu_j -})(\delta^{\mu_i +} \delta^{\nu_i +} - \delta^{\mu_i -} \delta^{\nu_i -})] S_i^{\nu_i} S_j^{\nu_j}, \end{aligned}$$

and defining

$$\zeta^{\mu\nu} := \delta^{\mu 0} \delta^{\nu 3} + \delta^{\mu 3} \delta^{\nu 0}, \quad \kappa^{\mu\nu} := 2\delta^{\mu +} \delta^{\nu +} - 2\delta^{\mu -} \delta^{\nu -},$$

one arrives at

$$\sum_{i \neq j} J_{ij} [S_i^3 S_j^3, S_i^{\mu_i} S_j^{\mu_j}] = 2 \sum_{i < j} J_{ij} \sum_{\nu_i \nu_j} [\zeta^{\mu_i \nu_i} \kappa^{\mu_j \nu_j} + (i \leftrightarrow j)] S_i^{\nu_i} S_j^{\nu_j}.$$

Note that we have used ν_i both for the eigenfrequencies and as a mute index, labeling $\{\text{Id}_i, S_i^+, S_i^-, S_i^0\}$. Its usage should be clear from the context.

The full evolution of the density matrix is given by

$$\partial_t C_{\mu_1 \dots \mu_N} = \sum_i \lambda_i^{\mu_i} C_{\mu_1 \dots \mu_N} + \sum_i 4Y_i \delta^{\mu_i 3} C_{\mu_1 \dots 0_i \dots \mu_N} - \frac{2i}{\hbar} \sum_{i < j} J_{ij} \sum_{\nu_i \nu_j} (\zeta^{\mu_i \nu_i} \kappa^{\mu_j \nu_j} + \kappa^{\mu_i \nu_i} \zeta^{\mu_j \nu_j}) C_{\mu_1 \dots \nu_i \dots \nu_j \dots \mu_N}.$$

This is a systems of 4^N partial differential equations. We solved it by matrix exponentiation, using the library for linear algebra with sparse matrices contained in SciPy(Python).